Catalytic fast pyrolysis of beetle killed lodgepole pine in a novel ablative reactor

Heather G. Wise

A thesis

Submitted in partial fulfillment of the

requirements of the degree of

Master of Science

University of Washington

2018

Committee:

Fernando Resende

Anthony Dichiara

Rick Gustafson

Program Authorized to Offer Degree:

The School of Environmental and Forest Sciences

University of Washington

Abstract

Catalytic fast pyrolysis of beetle killed lodgepole pine in a novel ablative reactor

Heather G. Wise

Chair of Supervisory Committee:

Fernando Resende and Anthony Dichiara

Bioresource Science and Engineering

As carbon dioxide levels in the atmosphere continue to rise, lignocellulosic biomass is further being investigated for their potential as a feedstock for alternative fuels. Beetle killed lodgepole pine (BKLP) is a lignocellulosic biomass that becomes hazardous from structural defects caused by an infection of the mountain pine beetle, prompting its need to be removed from the forest and repurposed. The fast pyrolysis of BKLP generates organic volatiles, and that condense producing a liquid oil (bio-oil). The bio-oil produced is incompatible with the current infrastructure because of its acidic, corrosive, and unstable nature associated to its high oxygen content. The high oxygen content also results in a low higher heating value as compared to gasoline. Here, we explore two different methods to target the production of aromatic hydrocarbons, which are gasoline additives. In the first method, we deposited palladium metal nanoparticles on the BKLP to produce more phenolic compounds that act as precursors to the

target aromatic hydrocarbons. The second method involved adding a catalytic upgrade reactor downstream of an ablative reactor to upgrade organic volatiles into aromatic hydrocarbons.

TABLE OF CONTENTS

List of Figures

List of Tables

INTRODUCTION

1.1 Biofuels

There is a growing need for the development of alternative fuels as the use of petroleum continues to raise a number of environmental concerns. Harvesting coal, oil, and natural gas is hazardous, destructive to the environment and known to release trapped carbon dioxide into the atmosphere. Carbon dioxide levels before the industrial revolution were reported to be at 280 ppm and readily maintained by the earth's natural cycles. Now levels are increasing exponentially to almost 400 ppm as of 2015 (Figure 1).[1]

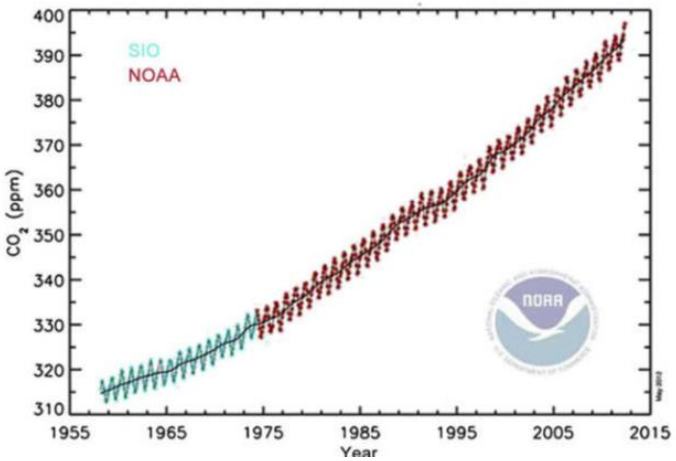

Figure 1.Monthly mean atmospheric CO^2 concentrations from Mauna Loa, Hawaii, sampling station. Data prior to May 1974 are from the Scripps Institution of Oceanography (SIO). Data since May 1974 are from NOAA/ESRL.[1]

The increased levels of carbon dioxide are affecting many of earth's natural ecosystems, putting them under stress and making alternative fuels a necessity. Biomass is a net zero carbon emission fuel source, because any carbon dioxide emitted in the creation or combustion of the fuel, would then be reabsorbed in the growth and life cycle of the tree. The development of biomass as a feedstock provides a significant positive environmental impact along with social and economic benefits that come with using a more sustainable feedstock. While methods exist to use food source

crops as feedstocks to create alternative fuels, lignocellulosic biomass is an alternative fuel source with many options for sustainable harvesting. Agricultural residues can be used as lignocellulosic feedstock as opposed to food source crops no longer contributing to the food versus fuel competition. Lignocellulosic biomass also tend to be more resilient to weather options, is available almost anywhere, and is a readily available waste, such as forest slash, from other process.

1.2 Beetle Infested Lodgepole Pine Trees

One example of lignocellulosic biomass that can be sustainably harvested is lodgepole pine (*Pinus contorta*) that has been infested by bark beetles, also called Beetle Killed Lodgepole Pine (BKLP). The mountain pine beetle is an insect originating from pine forests in western North America (British Columbia) and is known to find the lodgepole pine tree a desirable host. Traditionally the beetle has not spread beyond its historical location due to climate limitations in the surrounding area. However, as global climate continues to rise, and the harvesting of douglas fir and spruce increases, a high population density of lodgepole pine is left allowing the beetle to successfully cross boundaries not previously possible.[2] The bark beetle infested trees are creating problems for forest ecosystems, before the tree is dead. Once the trees are infected they begin to lose moisture content especially in the foliage, increasing the risk of wildfires that will spread quickly and burn more intensely through the canopy. As the foliage begins to fall, there is a decrease in canopy wildfire threat, and the tree enters the next degradation stage where debris from the tree accumulate on the forest floor, creating an opportunity for a more severe fire in the underbrush.[3] The dead trees need to be removed and repurposed to minimize the threat to forest ecosystems, and typical wood based manufacturing processes are not suitable for the damaged material. Within the first year of the initial attack, the tree experiences an 85% reduction in overall moisture content in the sapwood and heartwood, bringing the overall tree moisture content below the fiber saturation

point.[4] It is at this point that the tree becomes problematic for typical machining, as defects are more likely to occur below the fiber saturation point. Along with machining defects, blue fungi is often inoculated in the tree on the back of bark beetles, creating an undesirable blue discoloration in the wood that also makes it aesthetically unpleasing for uses in veneers or furniture.[4] As of 2011, there are 42 million acres of BKLP (1.U.S Forest Service, 2011) and the infection continues to spread. While typical wood industries have no use for this biomass, there are other processes that could break down the tree for its cellulose, hemicellulose and lignin monomeric units for alternative fuels. Applications include biochemical conversion for producing ethanol or xylitol and thermochemical conversion to produce specialty chemicals and fuels.[5,6] In order to understand the potential to use the biomass as a feedstock for other processes, the composition of the wood was determined. Luo et al. analyzed the wood in four different stages of tree degradation and determined that there is no statistical difference in wood carbohydrates, lignin, carbon, hydrogen, and oxygen contents between each stage.[7] Woo et al. also analyzed the overall sugar and lignin contents comparing a live lodgepole pine tree and a dead beetle infested tree, and found no significant difference in the lignin content with minor changes in carbohydrate content, primarily due to the digestion of hemicelluloses by blue fungi within the tree.[4] There is no direct effect of the beetle itself on the chemical makeup of the tree, meaning the that even the driest, and most digested material will still have the same amount of carbon available for conversion into fuel. Although the chemical makeup is unchanged, different conversion methods require different conditions and pretreatments to create high yields of alternative fuels. Biochemical conversion is commonly done using a pressurized steam system that requires the biomass to be saturated with water. BKLP has an incredibly low moisture content that would require more water to be added to the digester in order to reach the necessary pretreatment moisture content.[5] The method of

thermochemical conversion requires most of the biomass to be dried before use, to avoid waste of energy during the conversion of the biomass. The low moisture content innately provided by the beetle killed trees make those more suitable for thermochemical conversion for producing an alternative fuel.

1.3 Pyrolysis

Thermo-chemical conversion to a liquid fuel can be performed via pyrolysis, which is the heating of a substance in the absence of oxygen. The lack of oxygen prevents combustion from occurring, shifting the main products to char, condensable volatiles, and non-condensable gases, as opposed to purely carbon dioxide and water. There are two forms of pyrolysis, slow pyrolysis and fast pyrolysis, the difference between the two being the temperature of the process, the heating rate, and the length of exposure of the volatiles to high temperatures (residence time). Slow pyrolysis typically has heating a ramp time of 5-50 ℃/min, reaching 300-400 ℃ and the products are exposed to these conditions for minutes. The slow heat ramp primarily results in the formation of biochar. Fast pyrolysis temperatures are anywhere from 400-600 ℃ and this is achieved as quickly as possible (1000℃/min)[8], or the heat ramp is in the absence of the biomass, to minimize the formation of char, and maximize organic vapor yield. Vapors created from fast pyrolysis are exposed to these temperatures for less than a second to minimize secondary reactions between the volatile components.[9] The primary product from fast pyrolysis consists of condensable volatiles that form a liquid when condensed. This bio-oil product is valuable for the production of other chemicals, because of the different conversion methods available to refine this bio-oil into desired fuels and chemicals. The creation of these refined fuels and chemicals from fast pyrolysis condensable volatiles is the overall goal of this combined work.

1.4 Bio-oil

Bio-oil is a common name given to the mixture of different volatiles produced from biomass pyrolysis once they are condensed into a liquid. Cellulose, hemicellulose and lignin are the three primary polymers of biomass that break down during fast pyrolysis to form the mixture of condensable volatiles consisting of alcohols, acids, ketones, furans, anhydrous sugars, phenols, guaiacols, and aromatics. The bio-oil is very unstable because of the aldehyde and ketones (reactive groups) and has an acidic and viscous nature due to the high oxygen content, which is not compatible with existing infrastructure.[10] Cellulose and hemicellulose are often more readily broken down than lignin and produce mainly smaller compounds such as alcohols, acids, ketones, furans and anhydrosugars that make up a lighter fraction of bio-oil.[10,11,12] Lignin is a polymer with higher thermal stability and is typically more challenging to break down, resulting in the production of larger molecules like phenols, guaiacols, and aromatics that make up a heavy fraction of the oil.[13] The mixture of volatiles created is heavily oxygenated due to the large amount of oxygen in the three primary polymers, and while a liquid fuel is created, the quality is poor. The mixture of bio-oil compounds has a higher heating value (HHV) of 18-20 MJ/kg, which is significantly lower than comparable liquid fuels like diesel, gasoline, and heating oil with HHV's around 42-45 MJ/kg.[6] The undesirable qualities caused by the presence of oxygen could be improved by removing oxygen to produce hydrocarbons that more closely resemble the make up of gasoline. Gasoline is primarily made of four different molecular structures, iso-paraffins (~50%), olefins (~10%), and aromatics (~40%). Aromatics and polyaromatics tend to be the larger molecular compounds in gasoline and are a significant portion of the volume. The structure of the desired aromatics, such as toluene and methylated benzenes, very closely resembles the chemical structures naturally found in the monomeric units of wood polymers, such as lignin and cellulose.

The goal of this work is to transform these wood fast pyrolysis derivatives into desired aromatics, to create an alternative fuel from biomass that is compatible with current infrastructure.

1.5 Catalytic Upgrade

To transform the bio-oil volatiles produced from fast pyrolysis (primary reactions), we will upgrade them using a catalyst (secondary reactions). Catalytic fast pyrolysis is typically carried out using two different methods, *in-situ* or *ex-situ*, in which the location of the catalyst defines the method. The first method (*in-situ*) refers to the catalyst placement in the same reactor chamber that the fast pyrolysis occurs in, meaning the primary and secondary reactions occur simultaneously under the same conditions. The second method (*ex-situ*) involves placing the catalyst in a secondary chamber, and as the volatiles are formed in the primary reactor, they flow to the secondary chamber, usually via a heated transfer line, and undergo secondary upgrade reactions (Figure 2)[14].

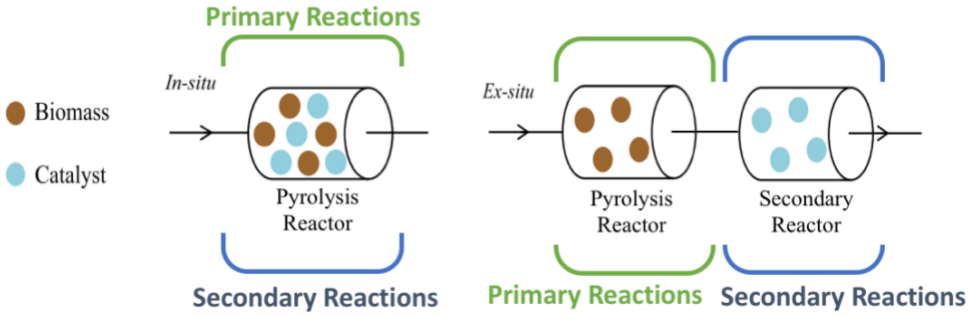

Figure 2. Diagram depicting in-situ and ex-situ methods of catalytic fast pyrolysis.

There are not many studies done comparing *in-situ* and *ex-situ* catalytic fast pyrolysis and most of the studies are conducted on a microscale. If we just consider overall yield of aromatics, most studies report that *in-situ* processes are more effective at creating aromatics.[15,12,16] However, if we compare the selectivity of aromatics created from these two different methods, we see that *ex-situ* methods are more selective to monoaromatic hydrocarbons, such as toluene and other methylated

benzenes, while *in-situ* techniques are more selective to producing large polyaromatic hydrocarbons.[16,15] Catalyst to biomass ratio is another parameter heavily influenced in the *in-situ* configuration of the catalyst, as opposed to the trends observed for *ex-situ configuration*. A high catalyst to biomass ratio is necessary to ensure all volatiles are exposed to active sites within the catalyst, but this causes a heat transfer limitation with increasing sample mass.[16] Alternatively, it has been shown that *ex-situ* can achieve similar yields at a lower catalyst to biomass ratio. *Ex-situ* also has the added benefit of being able to control pyrolysis temperature and the upgrade temperature of the catalyst separately to optimize each process and create the highest yield for a variety of catalysts.[16,14] While larger yields of aromatics are produced in the *in-situ* method, there are a number of other factors to consider, including reactor size, target compound, and reactor design before deciding on one or the other. These factors not only help to determine the method of catalytic fast pyrolysis but also the catalyst itself. Catalysts typically used in this process are silica aluminum based catalysts called zeolites. Zeolites are based off the same chemical building blocks of a silica tetrahedron or an alumina tetrahedron. This structure has an aluminum or silica atom stabilized by four oxygen groups and can be combined in different ways to form a variety of structures. The most commonly employed zeolite for deoxygenation of bio-oil to produce aromatics is HZSM-5. There have been comparative studies conducted against other zeolites, such as Y zeolite, activated alumina, H-Beta, etc. but HZSM-5 has the highest selectivity to deoxygenated aromatics like the ones we are targeting.[11,17]

1.6 Objective

We propose upgrading organic volatiles from fast pyrolysis using two different approaches. The first one consists of altering the biomass to promote the generation of desired aromatic hydrocarbons. The BKLP material will be modified by the addition of zero-valent palladium

nanoparticles and then tested on a microscale fast pyrolysis system to examine the effect of palladium on the formation of aromatic hydrocarbons. The second approach is to implement a lab scale *ex-situ* upgrade reactor downstream of an existing ablative fast pyrolysis unit to hold a catalyst and upgrade volatiles into the target product. The *ex-situ* reactor design was based off of data collected during *ex-situ* catalytic fast pyrolysis experiments conducted on the microscale.[16]

CHAPTER 2. Pyrolysis of beetle killed lodgepole pine decorated with palladium nanoparticles

2.1 Introduction

Fast pyrolysis is becoming an increasingly popular method for producing specialty chemicals and fuels from biomass, because of the high liquid yield referred to as bio-oil. Bio-oil is a complex mixture with a high acidity, viscosity, and instability resulting from the high oxygen content. These negative qualities demand a catalytic upgrade to improve the quality of the fuel and target hydrocarbons. Catalytic upgrade is commonly done in an *in-situ* or *ex-situ* method, where the catalyst is either placed in the pyrolytic chamber with the biomass (*in-situ*) or placed in a secondary downstream upgrade reactor (*ex-situ*).[15] The upgrade involves the deoxygenation of condensable volatiles using a variety of catalysts such as traditional zeolites (acid zeolites, metal zeolites) or more recent methods involving metal deposition on various supports, such as carbon nanotubes. The pore structure of the catalyst is as critical as its composition for the upgrade reactions. Zeolites are known to have problematic diffusion properties, as diffusing molecules are constantly in contact with channel walls, causing a high dependency on zeolite chemical structure, shape, size, and concentration of adsorbed species.[18] In zeolites with larger pore structure, smaller molecules experience a high diffusivity at lower concentrations, while smaller pore zeolites exhibit diffusivity

limitations with larger molecules.[11] In any zeolite structure the support is critical to the diffusivity and complications can arise from lattice defects, cation distribution, and pore shape and size. Carbon nanomaterials based catalysts such as metal impregnated carbon nanotubes also present similar challenges, as deposited particles can block primary pathways of diffusion for molecules.[19] Regardless of the use of the *in-situ* or *ex-situ* configuration, all of these problems can lead to an increase of coke on the catalyst, and limited access to active sites due to pore plugging effects, hence decreasing yields.[19] These problems led us to propose the removal of the complex support all together, discarding delicate diffusion processes and making the active site readily available for molecules to interact. The placement of active sites, in our case metal nanoparticles, directly on the surface of the biomass would allow for condensable volatiles to directly interact with a metal active site. Similar studies have been conducted with the placement of metal ions in biomass or lignocellulosic biomass polymers, and have demonstrated that fast pyrolysis of the modified material affects the decomposition.

Collard et al. investigated the effect of nickel and iron on the crystallinity index and their subsequent fast pyrolysis and used slow pyrolysis to help explain the possible mechanism. They found that metal ions interacted with the cellulose bonding producing more amorphous regions. The interaction of these metal ions catalyzed some decarboxylation reactions and stabilized the cellulose matrix making depolymerization more difficult and promoting the production of char and carbon dioxide.[20]

Xing et al. impregnated wood with copper and potassium ions and conducted slow pyrolysis using thermogravimetric analysis TGA, and fast pyrolysis in a Py-GCMS. They discovered that potassium has a different catalytic effect then copper. In slow pyrolysis, increasing the potassium concentration increased the extent of decomposition of lignin, while copper increased the extent

of decomposition of the cellulose. Fast pyrolysis showed that potassium favored the production of lignin derivatives as well as cellulose derivatives and copper favored the production of hemicellulose pyrolytic products.[21]

Dalluge et al. tested the effect of alkali and alkaline earth metal ions on the production of char and volatile aromatics from lignin. They found that alkali earth metals promote the production of volatile aromatics and char, as well as alter the cleavage of linkages within lignin.[22]

Here we placed reduced palladium metal nanoparticles on the surface of BKLP and conducted fast and slow pyrolysis to observe any catalytic effect the palladium nanoparticles may produce. Metal nanoparticle impregnation of woody biomass has previously not been done, because of the necessary thermal reduction step, that prematurely decomposed the wood. The use of metal nanoparticles rather than ions has been successful in catalytic deoxygenation of phenol, and also demonstrated a hydrogenation effect when placed on carbon nanotubes.[23,24] There are also studies conducted on the placement of metal nanoparticles such as rubidium on graphene for catalytic upgrade of bio-oil volatiles.[25] The placement of palladium nanoparticles, a proven deoxygenation catalyst, on the direct support of the wood itself could allow for deoxygenation of the bio-oil volatiles without the need for diffusion in and out of pores. It is also possible that the palladium could have an effect on biomass polymer decomposition. Lu et al. conducted catalytic fast pyrolysis of palladium and tungsten activated carbon used in an *in*-situ method saw that the use of noble metals like palladium and tungsten, result in an increase amount of phenolics produced from lignin.[26]

Chen et al. developed a new method for self-reducing palladium nanoparticles without use of extreme heat. It involves the natural reduction of palladium by lignin polymers within the biomass.[27] This study attempts to create a one-step upgrade in which deoxygenated aromatics are

produced, and simultaneously create some catalytic effect aiding the decomposition of any of the wood polymers, such as lignin, thus producing more aromatic volatile precursors.

2.2 Materials and Methods

2.2.1 Beetle Killed Lodgepole Pine

Two to four years past death Beetle killed lodgepole pine (BKLP) was purchased from Forest Concepts LLC. The provided sample was oven dried and ball milled to <200 µm and sieved using a size 300 mesh. Particle size distribution was determined by optical microscopy (Zeiss Axiolab) equipped with a CCD camera (Axiocam) using Image J software.

2.2.2 Preparation of palladium BKLP

BKLP was ball milled to reduce particle size and two different loadings of palladium wood (Pd Wood) were prepared at 1.0 and 1.5 target weight percent of biomass. Palladium wood (Pd wood) was prepared in 500 mg batches by mixing $PdCl_2$ (Alfa Aeasar, 99.9% purity) with 20 mM HCl (Fischer Scientific). The hydrochloric acid solution was refluxed at 80 ℃ and the $PdCl_2$ solution was added along with the ball milled BKLP. The mixture was stirred and maintained at 80 ℃ for 6 hours. The wood was then vacuum filtrated, rinsed with deionized water, and dried in an oven for 24 hours at 75 ℃.

2.2.3 Characterization

The palladium content was measured by inductively coupled plasma spectroscopy (ICP-MS, Perkin Elmer ELAN-DRCe). Palladium wood samples were digested using nitric acid and hydrogen peroxide (3:1 v/v) in a microwave digester using 1400 W for 30 min. Digested samples were then diluted to ppb levels and run through the ICP-MS. Digested sample counts were compared against a set of known standards created from palladium ICP-MS standards from Sigma Aldrich.

Scanning electron microscopy (SEM, XL830, FEI company, Hillsboro, OR , USA) was conducted at 5 kV on samples deposited on carbon tape and sputter coated with a thin layer of platinum. Elemental analysis was also conducted with an energy dispersive X-ray spectroscope (EDS) to determine a mapping of palladium content across the wood particles.

X-ray diffraction profiles of palladium-decorated wood were obtained with a Bruker D8 X-ray powder diffractometer using a Ni filtered Cu-Kα radiation generated at 40 kV and 40 mA. Palladium wood was pressed to a film before the measurement. Diffractograms were collected at a rate of 2 degrees/min from 10 to 90 degrees two theta. The Pd crystallite dimension of (111), (200), and (311) planes were calculated based on the Scherrer equation.[28]

2.2.4 Thermogravimetric analysis

TGA (PerkinElmer STA 8000, USA) was used to determine the performance and products generated from slow pyrolysis of the Pd wood. TGA experiments were conducted with a 5 mg sample at a heat ramp of 10 ℃/min to a final temperature of 800 ℃, in pure nitrogen. A combination TGA (TGA, PerkinElmer STA 8000, USA) -FTIR (PerkinElmer Frontier, USA) was used on a 14 mg sample with a heat ramp of 50 ℃/min to a final temperature of 900 ℃. As gaseous products were being produced from the slow pyrolysis, they were swept into the FTIR in pure nitrogen gas flowing at 50 ml/min through a heated transfer line maintained at 280 ℃. FTIR spectra were collected from 500 to 4000 cm^{-1}, with a resolution of 4 cm^{-1}, corresponding to scan intervals of 3 seconds.

2.2.5 Fast Pyrolysis coupled with gas chromatography, mass spectrometry and flame ionization detector (Py-GC/MS-FID)

Fast pyrolysis was conducted in a 5200 microscale pyrolyzer from CDS Analytical LLC. Each run consisted of a 0.5 mg sample of Pd BKLP that was placed in a quartz tube. Quartz wool was used

on both sides of the sample to secure its position during fast pyrolysis. The sample was placed inside a platinum coil and the coil was heated at a rate of 1000 ℃/min to a final temperature of 550 ℃ and maintained for 45 secs. The volatiles created from fast pyrolysis were then carried using helium gas at a flow rate of 50 ml/min directly to a GC/MS-FID (QP2010 Ultra, Shimadzu). through a heated transfer line maintained at 300 ℃ . Separation of compounds was achieved in a SHRXI-5MS capillary column (30 mm x 0.25 mm I.D. x 0.25 μm film thickness). Compounds from the transfer line entered an injector held a 300 ℃ with a split ratio of 30:1. The oven temperature began at 40 ℃ for 4 min and was raised to 300 ℃ with a heat ramp of 20 ℃/min, and then held at temperature for 5 min. All compounds were qualitatively determined using the mass spectra comparison with NIST 2010 library. All compounds were quantified using the peak area taken from the FID. This peak area was than matched against standard curves created for 40 oxygenated compounds and 15 deoxygenated compounds. In the event we collected a compound without an exact calibration, approximations were made using a compound of similar chemical structure. Yield and selectivity of compounds were reported using the following equations:

$$\%\, Yield = \left(\frac{Mass\ of\ compound\ i\ in\ products}{Mass\ of\ reacted\ biomass}\right) \times 100 \quad (1)$$

$$\%\, Selectivity = \left(\frac{Mass\ of\ compound\ i\ in\ products}{Mass\ of\ total\ observed\ products}\right) \times 100 \quad (2)$$

2.3 Results and Discussion

2.3.1 Characterization of BKLP

Characterization of the BKLP resulted in an average particle size of 34.2 μm (Figure 3). The small particle size resulted in a high surface area, allowing for high loadings of palladium and minimizing the risk of agglomeration of palladium nanoparticles. Ball milling the sample also

broke apart wood fibers and exposed the inner cell channels and pits, giving access for the palladium to penetrate throughout the wood particle, rather than just the outer surface.

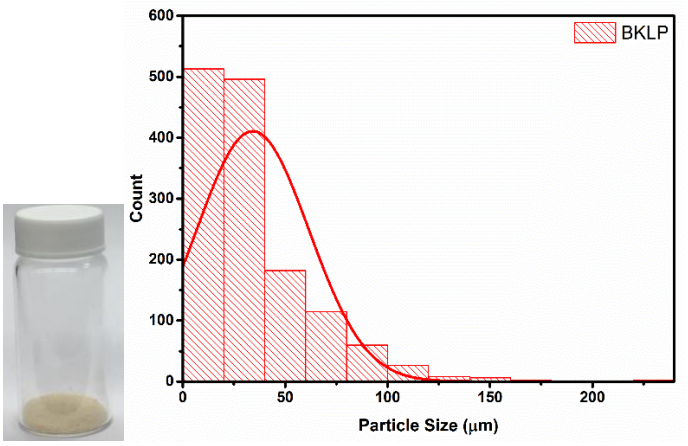

Figure 3. Image and normal distribution of ball milled BKLP particle size.

The particle size of palladium nanoparticles calculated using SEM and Image J software yielded a normal distribution with an average size of 13 nm and 16 nm for the 1.0 wt% and 1.5 wt%, respectively (Figure 4). This particle size determined through microscopy matched the particle size determined from the Scherrer equation (equation 3) and XRD data shown in Figure 5. Where B_{hkl} is average crystalline width, K is a constant that depends on the method of taking breadth (K = 0.9), λ is the wavelength of incident x-rays (λ= 0.15406 nm), θ is the corresponding bragg angle, and $\Delta 2\theta$ is the full width height minimum determined using OriginPro software. [28]

$$B_{hkl} = \frac{K\lambda}{\cos\theta \Delta 2\theta} \quad (3)$$

The average particle size determined from the Scherrer equation was 13 nm.

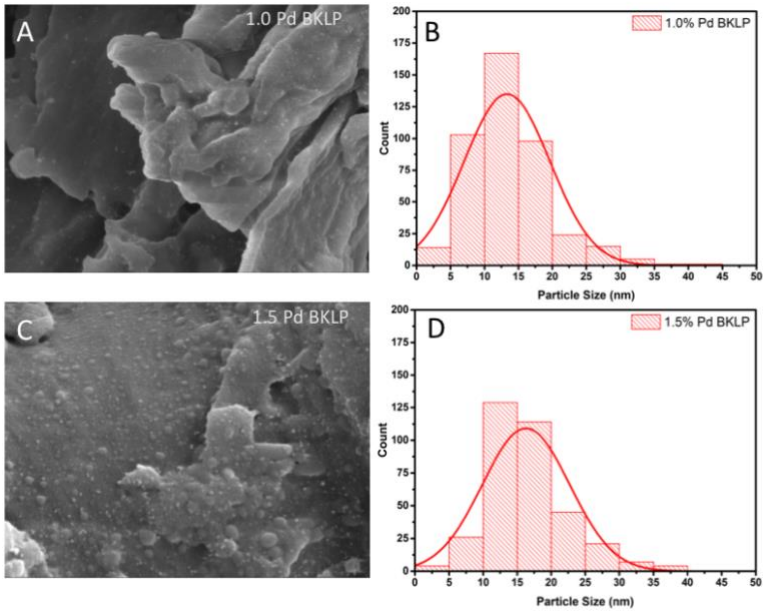

Figure 4. (A,B) SEM image and particle size distribution of palladium metal nanoparticles on BKLP at a 1.0 wt% loading. (B) SEM image and particle size distribution of palladium metal nanoparticles on BKLP at a 1.5 wt% loading.

Elemental Mapping revealed that the palladium is evenly distributed across the surface of the wood with minimal agglomeration. Point elemental analysis was done on specific points of the wood sample to approximate the palladium loading on both the 1.0 and 1.5 wt% revealing approximate loadings of around 2.0 % for both samples. ICP-MS was conducted on the two prepared Pd loadings as well as just BKLP to get a more representative idea of the true sample loading. The unimpregnated BKLP sample resulted in no significant amount of palladium and the 1.0 and 1.5 wt% loading resulted in 1.06 and 1.46 wt% respectively. The calculated loadings were similar to the target, suggesting that almost all the available palladium was deposited on the surface of the wood.

After the loading of palladium on the wood was determined, analysis was done to ensure the palladium was reduced. The reduction of palladium is necessary as this leads to the most active nanoparticle phase. The palladium impregnated sample exhibited a color change from a light brown to a dark brown color indicating the palladium was deposited on the surface of the wood.[29]

XRD of the palladium impregnated sample in Figure 5 showed palladium crystallographic phases Pd (111), Pd (200), Pd (220), and Pd (311). These phases are commonly associated with zero-valent palladium nanoparticles.[30]

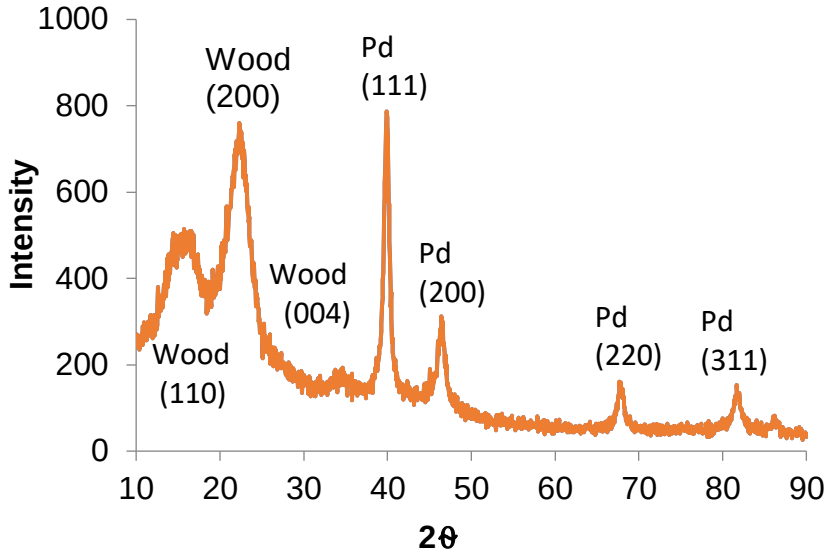

Figure 5. XRD of palladium wood sample.

Chen et al. claimed that the hydroxyl groups on the lignin are responsible for the reduction of the palladium nanoparticles, and there have been other reports of natural phenolics used in metal nanoparticle reduction steps.[30,31] FTIR spectra of plain BKLP were taken and compared to the two palladium-decorated samples, as shown in Figure 6.

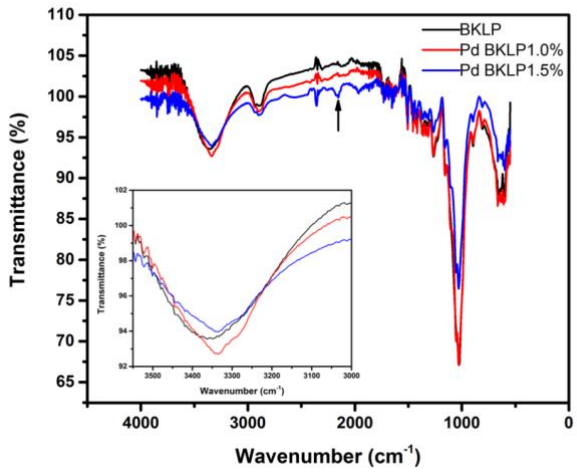

Figure 6. FTIR spectrum of BKLP, 1.0 wt% Pd wood, and 1.5 wt% Pd Wood with an inset showing details of red shift between 3000 to 4000 cm^{-1}.

Comparing the different spectra, a red shift was observed in the peak present between wavenumbers 4000 cm^{-1} and 3000 cm^{-1}. The peak shown at this range for the BKLP is likely representative of unbonded -OH groups on cellulose fractions that is exhibiting some intramolecular forces.[32] The palladium loaded samples show a red shift suggesting that the palladium metal nanoparticles are interacting with the hydroxyl groups on the cellulose, thus shifting the wavenumber. The reduction by the lignin within the wood and the interaction of the palladium nanoparticles with the cellulose suggested by the FTIR show the metal is interacting with wood polymers, especially the lignin because of the phenolic reduction, and possibly some with the cellulose as well.

2.3.1 Thermogravimetric Analysis (TGA)

We conducted TGA of pristine BKLP and the two prepared loadings (1.0 wt% and 1.5 wt%) to observe any catalytic effect the palladium might have on the decomposition of the wood. The TGA graph (Figure 7A) shows two major mass loss peaks at approximately 100 ℃ and 360 ℃. The first peak is due to the loss of water from the sample, and the second is associated with the decomposition of the wood polymers. At 800 ℃, the mass remaining was calculated and the weight

of the palladium was subtracted to determine the amount of BKLP char remaining (Table 1). The lowest loading of palladium (1.0 wt %) showed no significant decrease in the remaining char compared to the BKLP. This indicates that the 1.0 wt % palladium loading % was likely not high enough to have a significant effect on the decomposition of the biomass. However, the 1.5 wt% loading showed a significant decrease in char from 17.53% to 12.98%, indicating that the 1.5 % palladium loading was high enough to have a significant effect on the decomposition of the wood.

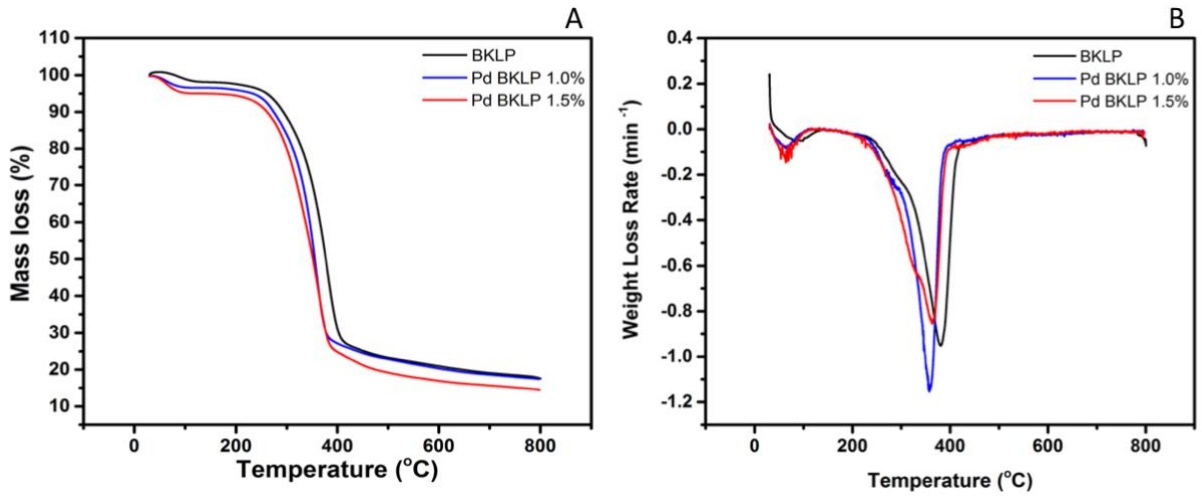

Figure 7. (A) TGA of BKLP and two prepared Pd Wood loading of 1.0 wt% and 1.5 wt% (B) DTGA of TGA of BKLP and two prepared Pd Wood loading of 1.0 wt% and 1.5 wt%.

Table 1. Peak position temperature values taken from the DTGA and remaining char from the TGA graph.

SAMPLE	PEAK POSITION (℃)	% CHAR
BKLP	380.59	17.53
Pd BKLP 1.0 %	363.72	16.36
Pd BKLP 1.5 %	357.86	12.98

Through the DTG graph (Figure 7B) we also see evidence of a catalytic effect from the presence of the palladium nanoparticles. The primary peak temperatures taken from the graph reveal that all samples with palladium show a decrease in peak temperature. As the palladium loading

increases, we see further decreases in the peak temperature greater than 20 ℃. TGA and DTG curves have been used to calculate activation energies of pyrolysis, and it has been shown that a decrease in DTG peak temperature is correlated with a decrease in activation energy.[21,33] The presence of the palladium has a catalytic effect, lowering the activation energy required to decompose cellulose, hemicelluloses and lignin, and shifting the temperature of decomposition to a lower value. The lower activation energy would also lead to further decomposition in the wood and thus decrease the residual char, consistently with the TGA data.

2.3.2 TGA-FTIR

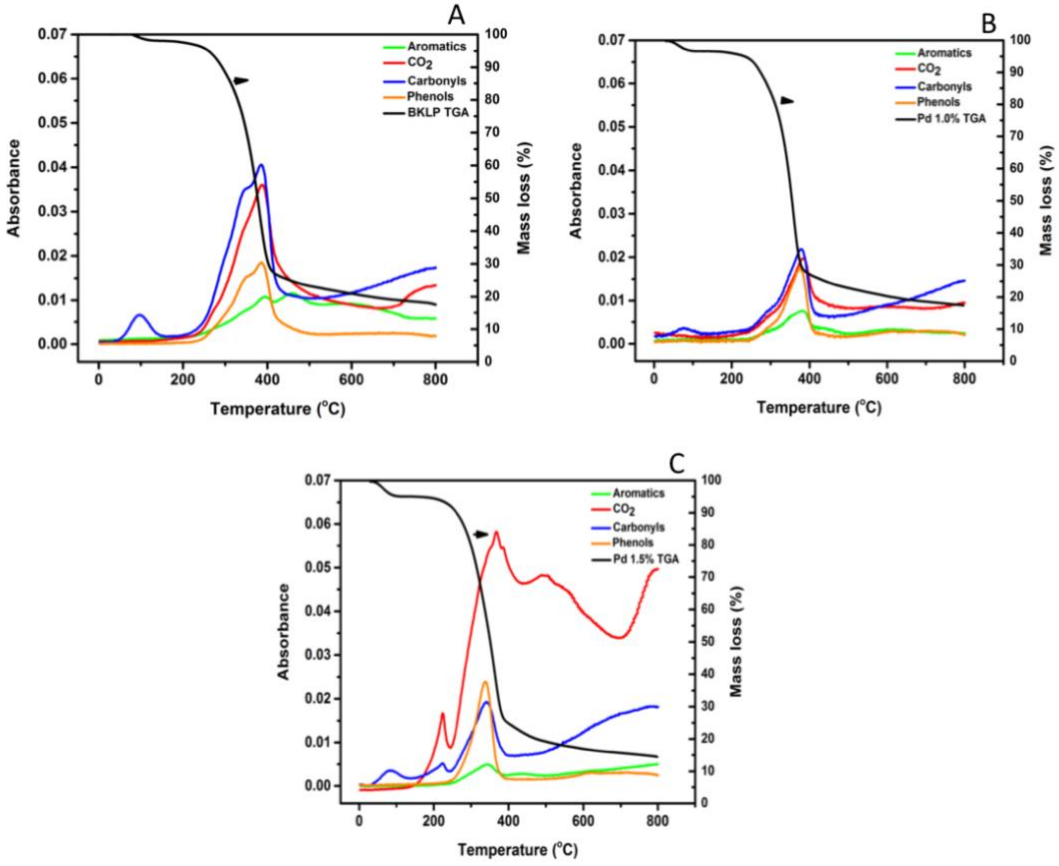

Figure 8.Combination TGA-FTIR plots of (A) blank BKLP, (B) 1.0 wt% Pd Wood and (C) 1.5 wt% Pd Wood.

TGA-FTIR was conducted to better understand how the palladium influences the decomposition of specific wood polymers by measuring products created from their slow pyrolysis and comparing them with the slow pyrolysis of unimpregnated wood.

Wavenumbers were chosen based on significant changes in compound absorbance when comparing the three prepared samples, since variations at other wavenumbers were considered insignificant. Comparing the BKLP and the palladium loading at 1.0% showed no significant increase in the production of phenols, and a significant decrease in the production of carbonyls and carbon dioxide (Figure 8 A,B). The BKLP compared to the 1.5% loading shows a significant increase in the carbon dioxide production and phenols with a significant decrease in carbonyls (Figure 8 A,C). We hypothesize that the decrease in carbonyls and carbon dioxide production in the 1.0% specimen is attributed to the palladium interaction with cellulose hydroxyl groups seen in the FTIR. The presence of the palladium metal could be inhibiting depolymerization of the cellulose.[20] An inhibition in the depolymerization of cellulose would likely result in the decrease of overall gaseous yields such as carbon dioxide. It is likely that the 1.0 wt % loading is too low to have an significant effect on the lignin as the phenols, which are common lignin derivatives, remain the same. The 1.5% loading showed a significant increase in carbon dioxide and phenol production suggesting that the palladium at a high enough loading catalyzed the breakdown of lignin into phenols and carbon dioxide. The decrease in carbonyls at the highest loading, could again be related to the interaction of the palladium with the cellulose inhibiting depolymerization, thus reducing the carbonyl yields. We expect the interaction with the lignin to be more significant as the hydroxyl groups are directly interacting in the reduction of the palladium nanoparticles. The temperatures in which the phenolic compounds are produced shifts to lower values, indicating that the palladium does have a catalytic effect on the decomposition of lignin, allowing this

thermally stable polymer to begin decomposing at a lower temperature. The prolonged carbon dioxide production at the 1.5% is likely due to the increased decomposition of lignin over time.

2.3.3 Fast Pyrolysis using a Py-GC/MS/FID

Fast pyrolysis was conducted in helium at atmospheric pressure and 550 ℃, using a micro-pyrolyzer in combination with a GC-MS/FID. We pyrolyzed BKLP and a single loading of 0.2 wt% Pd BKLP. The addition of palladium metal nanoparticles resulted in no significant increase of any hydrocarbons. There was a significant decrease in the production of alcohols, acids, ketones, and furans with the addition of palladium, suggesting that the metal nanoparticles are also inhibiting the depolymerization of cellulose during fast pyrolysis (Figure 9).[20]

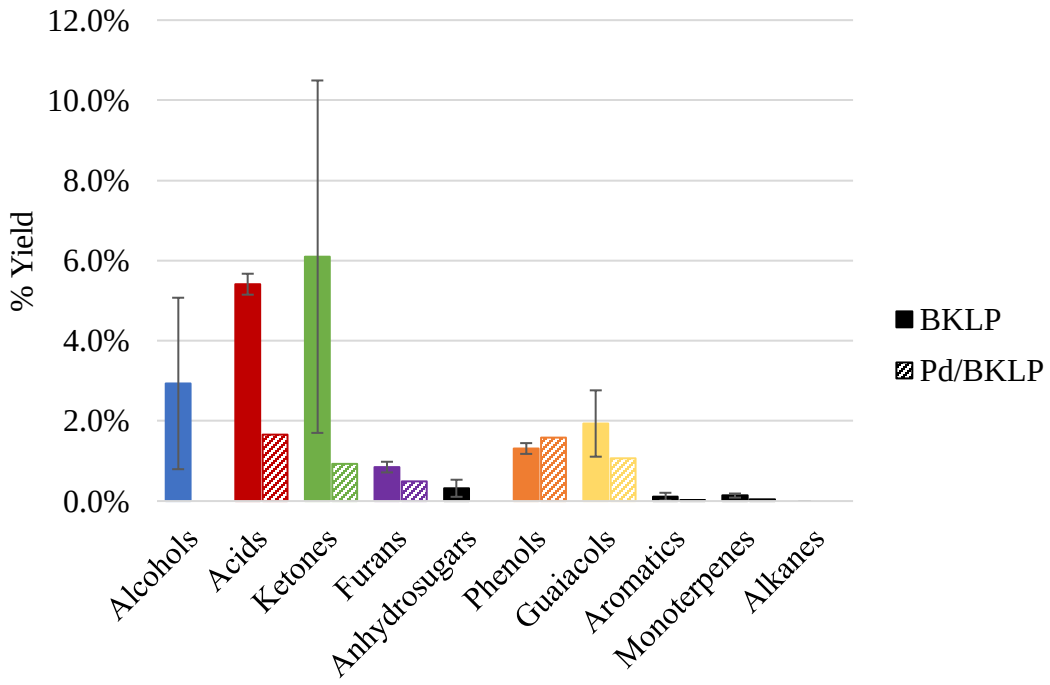

Figure 9. Yield of various compounds collected from Py-GC/MS-FID of unimpregnated BKLP(BKLP Ave and Pd BKLP.

Examination of the chromatogram (Figure 10) reveals that the most significant differences are the three peaks appearing at the later retention times associated with lignin pyrolysis products.

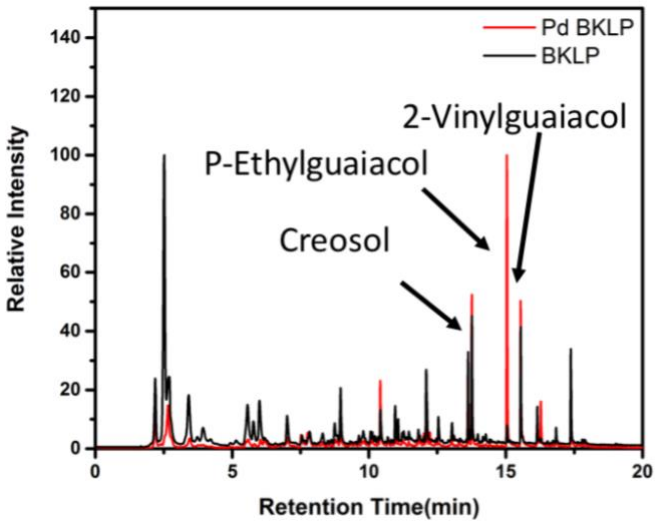

Figure 10. Chromatogram produced from fast pyrolysis of BKLP and Pd BKLP using a Py-GC/MS-FID.

While there is no significant increase in the yield of phenols and guaiacols, overall there is a significant increase in the selectivity of these compounds (Figure 11).

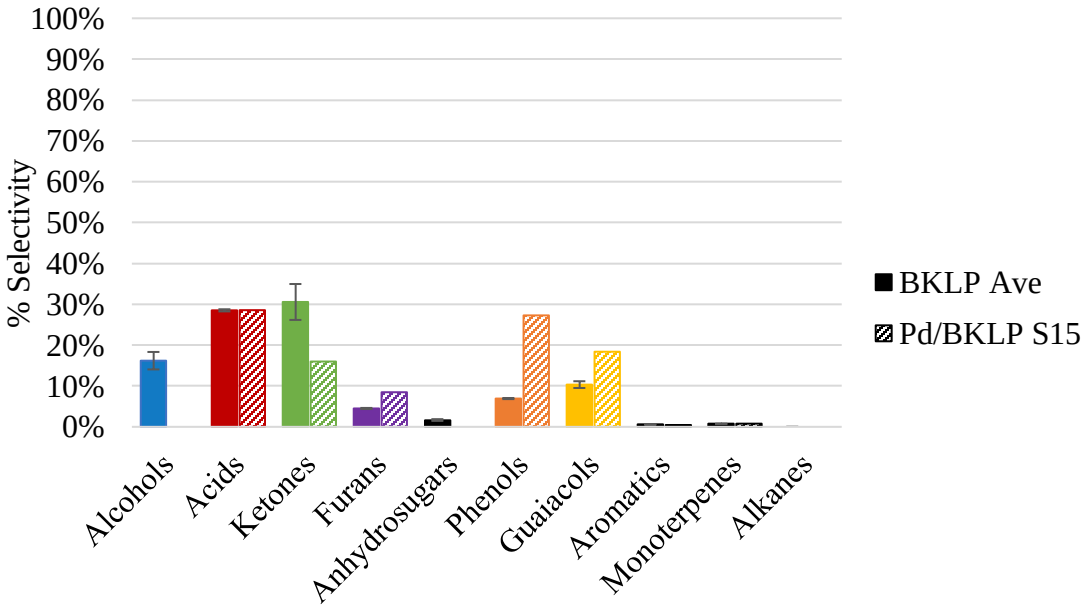

Figure 11. Selectivity of chemical groups produced from fast pyrolysis of BKLP and Pd BKLP.

Specifically, the selectivity and yield of creosol, p-ethylguaiacol, and 2-vinylguaiacol increase drastically, with the largest increase in p-ethylguaiacol (Figure 12). These three products have some commercial interest as well, for example, creosol is commercially used as a surfactant as well as a fungicide and preservative on telephone poles and railroad ties.

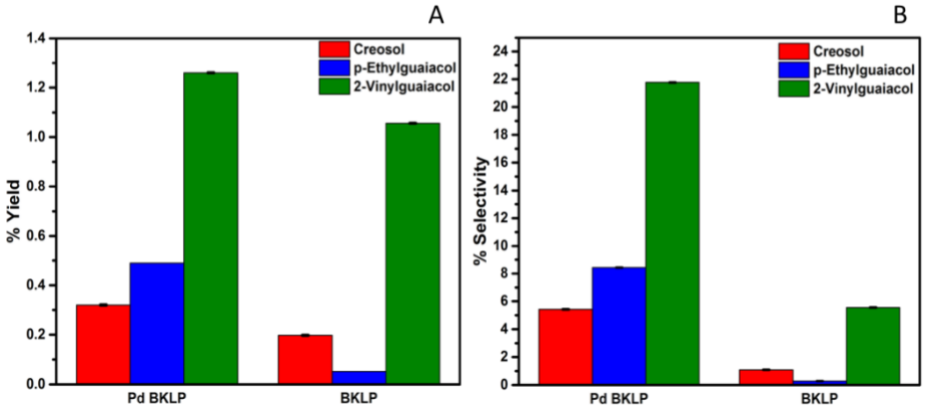

Figure 12. Yield (A) and Selectivity (B) of creosol, p-ethylguaiacol, and 2-vinylguaiacol produced from fast pyrolysis of BKLP and Pd BKLP.

This demonstrates the catalytic effect that the palladium has on the decomposition of the lignin by promoting production of lignin monomers. While no significant increase in the yield of deoxygenated products was observed, the increase in selectivity to phenol and guaiacols is significant in the contribution to target deoxygenated aromatics, as these are considered precursors to benzene, xylene and toluene. The addition of a catalyst in the *ex-situ* system described could result in an overall increase in deoxygenated aromatic volatiles.

CHAPTER 3: Ex-situ catalytic fast pyrolysis in a novel ablative reactor

3.1 Introduction

There are a variety of reactors used to conduct fast pyrolysis and produce bio-oil, the most common being a bubbling fluidized bed. There are a number of auxiliary costs associated with biomass pyrolysis, and they continue to present a problem with the economic viability of producing bio-oil. Process costs are elevated in biomass transportation, particle size reduction, and drying. A fast pyrolysis reactor that reduces some of these auxiliary costs would allow for this money to be used on a potential upgrade to bio-oil downstream, increasing the economic viability of the process. We have developed a reactor and chosen a feedstock to help reduce the auxiliary costs associated with pyrolysis, by taking advantage of the concept of ablative pyrolysis. Ablative pyrolysis involves the fast pyrolysis of a material primarily at the surface, making the fast pyrolysis process independent of biomass particle size. We applied this concept in our reactor design, which consists in a hot plate compressing on rotating biomass (Figure 13). In addition, we envision that this pyrolysis unit can be modified to operate as a mobile unit. This mobile unit could be transported to the forest and the biomass harvested and transformed into a high energy density bio-oil to be transported, avoiding the costs of transporting the lower energy dense biomass. The last problem of biomass moisture content is solved with the use of BKLP as the biomass feedstock. The infection and death of the tree results in dead and very dry biomass, in such a way that the use of this feedstock does not require extra energy for drying. This novel ablative pyrolysis reactor is functional and can produce a yield (equation 1) of bio-oil up to 60%, with the added benefit of decreasing costs in transportation, biomass pre-sizing, and drying.

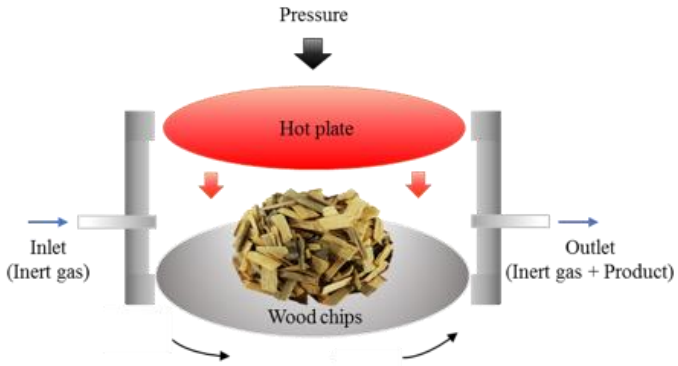

Figure 13. Concept design of the ablative fast pyrolysis unit. Nitrogen gas enters and a hot plate compresses on a rotating bowl containing wood chips. Volatiles are formed and swept out of the chamber.

While the bio-oil yield is high, the problem of bio-oil quality still holds true for this reactor, and an upgrade of some form is required to produce a fuel that is more readily compatible with the existing infrastructure. For this reason, we have developed a catalytic reactor downstream of the ablative fast pyrolysis reactor to upgrade volatiles in the gaseous phase as they are being produced. We have chosen an *ex-situ* system as opposed to an *in-situ* system for a variety of reasons. *Ex-situ* allows for individual temperature control of both the pyrolysis and the catalytic upgrade. *Ex-situ* also produces less carbonaceous residues. There are studies that show *ex-situ* has a higher selectivity than *in-situ* to monoaromatic hydrocarbons, our target product.[16]

There has been little work done in lab scale fast pyrolysis and followed by the subsequent upgrade of those fast pyrolysis volatiles to produce aromatic hydrocarbons. Almost all existing work is done *in-situ* and any existing *ex-situ* work has been conducted on a microscale, uses a co-feed of a hydrogen containing compound, or a model compound for the feedstock. B lui. Et al conducted a technoeconomic analysis of *in-situ* versus *ex-situ* pyrolysis, and claimed there is too little information on *ex-situ* catalytic pyrolysis to use actual data for an economic comparison. Instead, values were estimated based off of *in-situ* experiments.[34]

Huo et al. conducted bench scale fast pyrolysis with an *ex-situ* upgrade using 4 g of biomass and HZSM-5 as the catalyst. They tested a number of parameters and found that increasing temperature yielded a higher selectivity to aromatics and olefins, decreased coke, and char formation. The best result was a 21.7 % Carbon yield of olefins and aromatics (~10 C% aromatics) , collected at a fast pyrolysis temperature of 550 ℃, with an upgrade temperature of 600 ℃. They also observed a change in selectivity favoring benzene at higher *ex-situ* temperatures instead of methylated benzene rings.[34]

Mante et al. conducted an even larger pilot scale *in-situ* catalytic fast pyrolysis study in a circulating fluidized bed and collected approximately 10.9 wt% of the raw biomass fed in bio-oil (~29 gallons). The system included a catalyst (γ-Al_2O_3) and yielded around 5.42 wt% raw biomass in hydrocarbons. While the mass of biomass used in the run is significant, the study is difficult to compare to because it is performed *in-situ* and used a different catalyst.[35]

Shafaghat et al. conducted bench scale *in-situ* catalytic fast pyrolysis on 50 g of lignin with HZSM-5 in a bench scale fixed bed reactor. This study is close in feed size to what we are conducting with the same catalyst, however, they only use a fraction of the biomass polymers rather than the whole biomass. Using HZSM-5, they collected an approximately 2 wt% aromatic hydrocarbons yield from the lignin.[36]

Here, we conduct lab scale ($\leq$50 g of biomass) *ex-situ* catalytic fast pyrolysis using a packed bed upgrade reactor downstream of a novel ablative fast pyrolysis unit, to create monoaromatic hydrocarbons for use in alternative fuels.

3.2 Materials and Methods

3.2.1 Ablative Fast Pyrolysis

The ablative reactor includes a heated plate compressing on the surface of 50 g of BKLP 2-4 years past death (purchased from Forest Concepts LLC), chipped to 10 x 20 mm size sitting in a rotating bowl. Operating parameters were determined through previous screening experiments on the same reactor (Table 2).[37]

Table 2. Operating parameters for the ablative fast pyrolysis unit, determined through previously conducted screening experiments.

Parameters	**Set Point**
Fast Pyrolysis Temp	550 ℃
Pyrolysis Duration	3 minutes
Bowl Rotation	120 RPM
Nitrogen Flow	15 SLPM + Building Vacuum

The walls of the reactor are maintained at 300 ℃ to prevent condensation of organic volatiles. The system was modified from its previous configuration to accommodate the *ex-situ* upgrade reactor as well as an appropriate collection system for aromatic hydrocarbons (Figure 14).

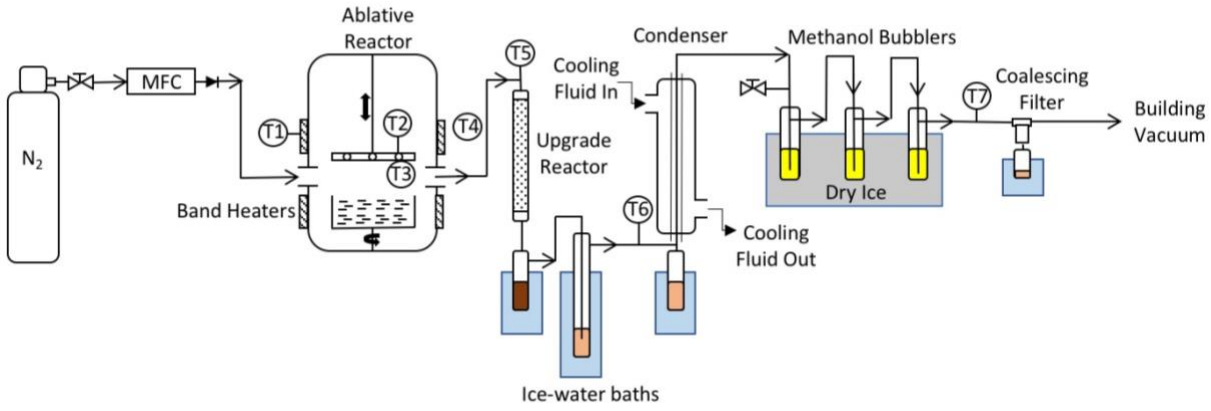

Figure 14. Flow diagram for ablative fast pyrolysis system, modified to accommodate an ex-situ upgrade reactor and collection system for aromatic hydrocarbons.

The system begins with a nitrogen tank and mass flow controller that allows the desired flow of nitrogen (15 SLPM) into the ablative system. In the ablative reactor, the wood is pyrolyzed and then volatiles are swept out of the chamber by use of a vacuum at the end of the system (building vacuum), through a heated transfer line maintained at 300 ℃, to prevent condensation of products, into the upgrade reactor. The upgrade reactor was designed from microscale experiments conducted on *ex-situ* fast pyrolysis of BKLP to accommodate a catalyst to biomass ratio of 5:1, as the results were not significantly different at higher ratios. The catalyst used in these microscale experiments was a powder form of HSZM-5 with a bulk density of 0.706 g/ml. From this bulk density, we determined the volume necessary to achieve a 5:1 ratio using 50 g of biomass, which was approximately .350 L. We designed the reactor to be approximately 0.340 L (Figure 15A). A wire mesh was tack welded at the one end of the reactor and the catalyst was packed with quartz wool at each end for support (Figure 15 B).

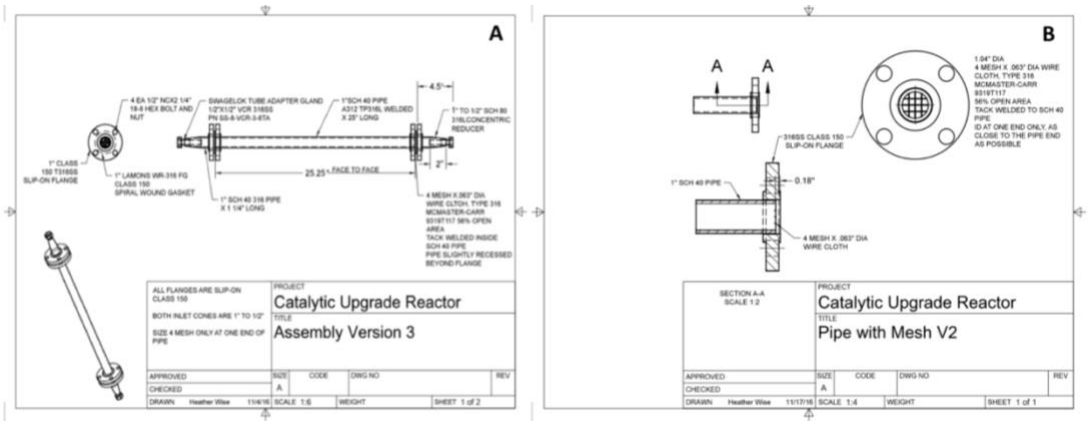

Figure 15. (A) Design drawings of ex-situ upgrade reactor with dimensions. (B) Cross section drawing of upgrade reactor and inset welded mesh for catalyst support.

The temperature of the transfer line leading to the upgrade reactor, and the temperature of the catalyst were controlled using K type temperature controllers and maintained at target temperature within plus or minus 10 ℃ . After the upgrade reactor, the volatiles pass through a collector submerged in ice, an impinger in an ice bath, and a double-pipe condenser with chilled propylene glycol flowing at -10 ℃, with an ice bath collector at the bottom to collect bio-oil running down the inner walls of the condenser. Any volatiles that did not condense in the condenser then flowed into three bubblers submerged in dry ice and filled with methanol. At the end of these methanol bubblers was a coalescing filter to collect any volatiles that had not condensed in the collection system and one last ice bath collector, followed by an outlet that was attached to a vacuum. Temperatures were collected at different points throughout the process and the averages are listed in Table 3.

Table 3. Average temperatures at each thermocouple in the ablative system.

Thermocouples	Temperature (℃)
T1	300
T2	300
T3	550
T4	300
T5	300-550*
T6	25 - 41**
T7	-4 - 10**

*Temperature of upgrade reactor varied
**This temperature is dependent on the temperature of the upgrade reactor

Most experiments were conducted using a building vacuum to help remove volatiles from the reactor chamber, making the collection of non-condensable gases impossible. To evaluate the yield of non-condensable gases, one experiment was conducted with a vacuum pump that allowed gases to be collected after the vacuum, for further analysis of non-condensable products and closure of mass balance.

3.2.2 Analysis of Products

Products were collected from all collection points (3 ice bath collectors, 3 dry ice methanol bubblers, and 1 dry ice collector), dissolved in methanol, and ran through a GC/MS-FID (QP2010 Ultra, Shimadzu). Separation of compounds was achieved in a SHRXI-5MS capillary column (30 mm x 0.25 mm I.D. x 0.25 μm film thickness). The GC inlet temperature was 300 ℃ with an inlet split ratio of 30:1. The oven temperature began at 40 ℃ for 4 min and was raised to 300 ℃ with a heat ramp of 20 ℃/min, and then held at temperature for 5 min. All compounds were qualitatively determined using the mass spectra comparison with NIST 2010 library. All compounds were

quantified using the peak area obtained from the FID. This peak area was than compared against standard curves created for 40 oxygenated compounds and 15 deoxygenated compounds. In the event we collected a compound without an exact calibration, approximations were made using a compound of similar chemical structure. Yield and selectivity of compounds were reported using equations 1 and 2.

An elemental analyzer from Perkin Elmer (series II 2400) was used to determine carbon content left on the spent catalyst and in the bio-oil as well. Approximately 5 mg of oil was used for each liquid sample, and approximately 20 mg of spent catalyst to determine the amount of carbon.

Non-condensable gases were collected during one run and analyzed on a GC/TCD-FID with a SUPELCO 60/80 Carboxen-1000 packed column (4.6 m x 2.1 m I.D. x 0.5 μm film thickness). Helium with a flow rate of 35 ml/min was used as carrier gas. The oven began at a temperature of 40 ℃ for five minutes and was then ramped up to 225 ℃ at a rate of 20 ℃/min, and then held at temperature for 10 min. Compounds were compared against known standards for quantification and matching retention times were used for qualification of compounds. Calibration compounds include 60 different compounds composed of a variety of acids, ketones, aldehydes, furans, guaiacols, phenols, anhydrosugars, monoterpenes, substituted aromatic hydrocarbons, alkanes, and alkenes.

3.2.2 Catalyst

The catalyst used in experiments was a mostly microporous pelletized HZSM-5 with a silica to aluminum ratio of 38. BET (Micrometrics, TriStar II PLUS) was conducted on fresh and spent catalyst to understand how the coke formation affected the surface area and pore volume; samples

were degassed at 150 ℃ for 24 hours. Unreacted catalyst was heated under nitrogen to replicate the conditions during pyrolysis and found to have a surface area of 275 m^2/g.

3.3 Results and Discussion

3.3.1 Effect of Temperature

A single run produces light oil, heavy oil, char, and coke at different collection points, and the multistep collection system provides a clean separation. Light oxygenated oils and water are almost exclusively left in the three ice bath collectors, heavy oils and char remain in the reactor, while coke remains in the upgrade reactor, and aromatic hydrocarbons are exclusively collected in the methanol bubblers. The aromatic hydrocarbons are the most valuable part of the yield for the production of alternative gasoline compounds and were considered part of the light oils in the mass balance. Mass balances were as high as 82 % excluding non-condensable gases (Figure 16). Assuming that the remainder of the mass not accounted for are non-condensable gases, the significant decrease in mass balance from 400 ℃ to 450 ℃ could be a result of increased extent of deoxygenation and thermal cracking, resulting in more non-condensable gases. That drop is not observed at 550℃ because the mass balance closure at that temperature includes approximately 13% non-condensable gases. There is no significant effect of upgrade temperature on the char and heavy oil, as it is to be expected as fast pyrolysis conditions remained the same

across all runs, and char and heavy oil were collected only in the ablative reactor. The varying light oil yield could be due to light oil collection error.

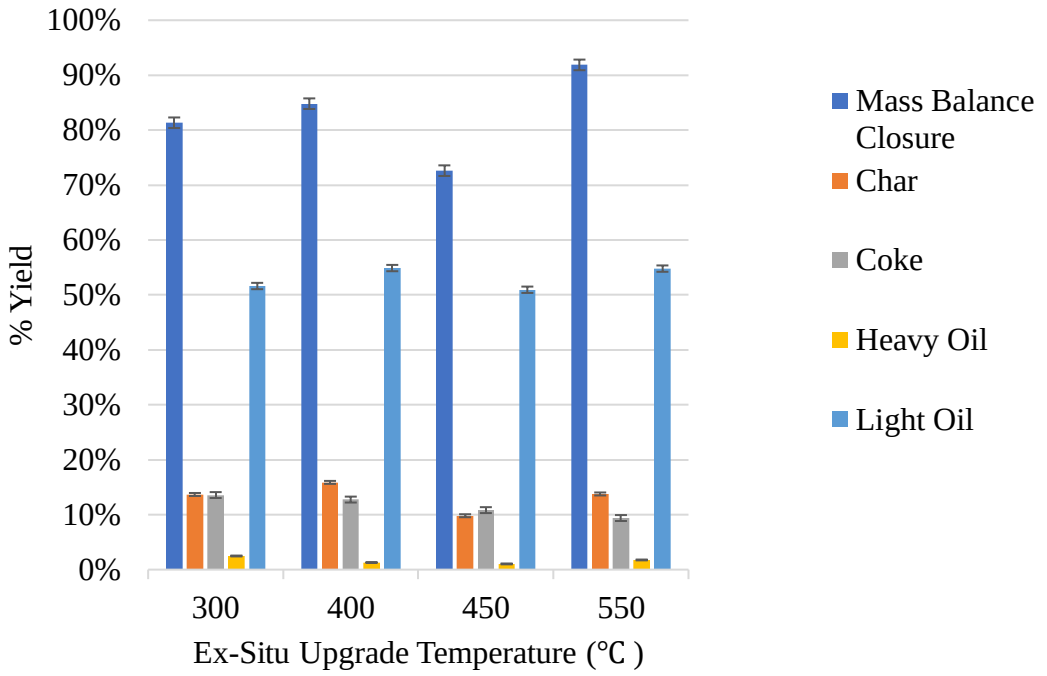

Figure 16. Mass balance breakdown of all solids and liquids collected from the conducted temperature study.

*Upgrade temperature 550 ℃ includes single non-condensable gas run

We conducted a study on the effects of temperature to understand how the *ex-situ* upgrade reactor temperature affects the aromatic hydrocarbon yield. For the temperature screening, the ablative reactor was operated at the conditions outlined in Table 2, and the upgrade reactor was loaded to a catalyst to biomass ratio of 4:1 (~200 g of catalyst). Temperatures were varied from 300 ℃ to 550 ℃ (Figure 17), temperatures higher than 550 ℃ were attempted, but unsustainable using the heating tapes and equipment available.

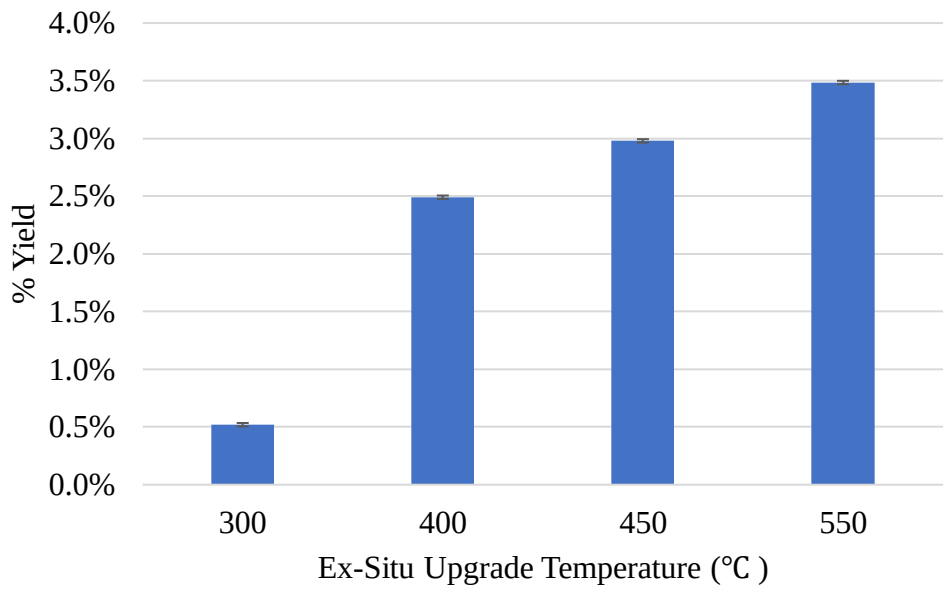

Figure 17.Yield of aromatic hydrocarbons as a function of ex-situ reactor temperature.

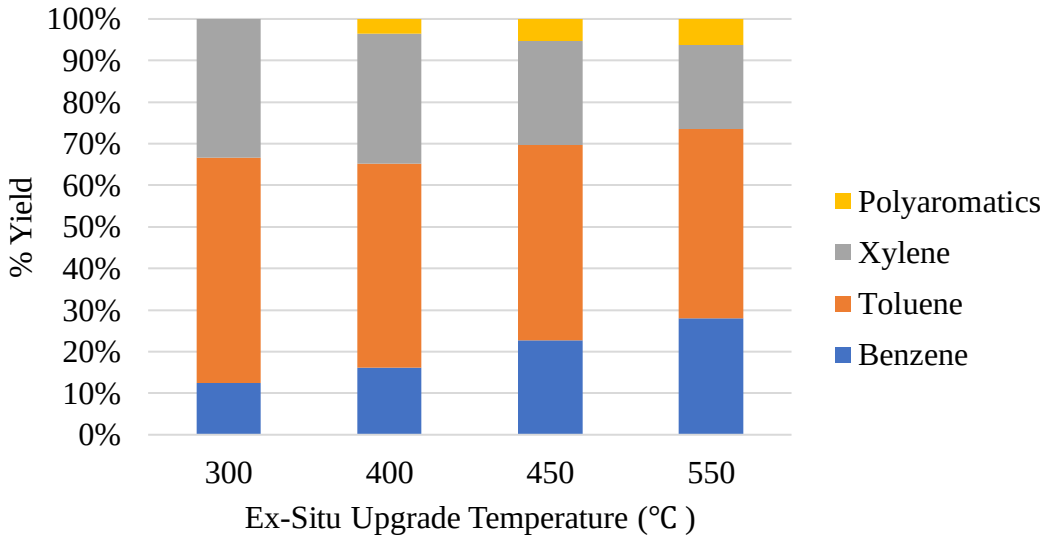

Figure 18. Selectivity of aromatic hydrocarbons as a function of ex-situ reactor temperature.

As temperature increased, the yield of aromatic hydrocarbons increased significantly, reaching the highest yield of 4.3 % at 550 ℃. This trend of increasing aromatic hydrocarbon yield with temperature for HZSM-5 is consistent with trend reported in the literature.[12,17,19] The aromatic hydrocarbons being produced were all monoaromatic hydrocarbons, and exclusively benzene,

xylene and toluene (Figure 18). As temperature increased, we observed a change in the selectivity of monoaromatic hydrocarbons. Increasing temperature produced more benzene and polyaromatic hydrocarbons, with less xylene, while the toluene exhibited no significant difference. We hypothesize that the selectivity to benzene increased as the temperature increased because of secondary thermal cracking.[15,11] As methylated benzene rings are exposed to higher temperatures, the possibility of thermal cracking increases, increasing the probability of demethylation, resulting in more benzene rings and less methylated benzenes such as xylene. This is consistent with trends observed in microscale ex-situ experiments conducted by G. Luo, as *ex-situ* temperature increased monoaromatic hydrocarbons increased.[16] There was also a significant increase in polyaromatic hydrocarbons from 300 to 600 ℃ in these microscale experiments which is consistent with the trend of increasing selectivity to in polyaromatic hydrocarbons seen here . This increase is suggestive of secondary polymerization reactions occurring or the promotion of desorption of larger aromatic hydrocarbons from the catalyst. This idea of thermal cracking and increased coke desorption is also supported by catalytic coke trends (Figure 19). Using the CHN, we determined the mass of coke left on the catalyst and assumed all coke was deoxygenated and only consisted of carbon and hydrogen.

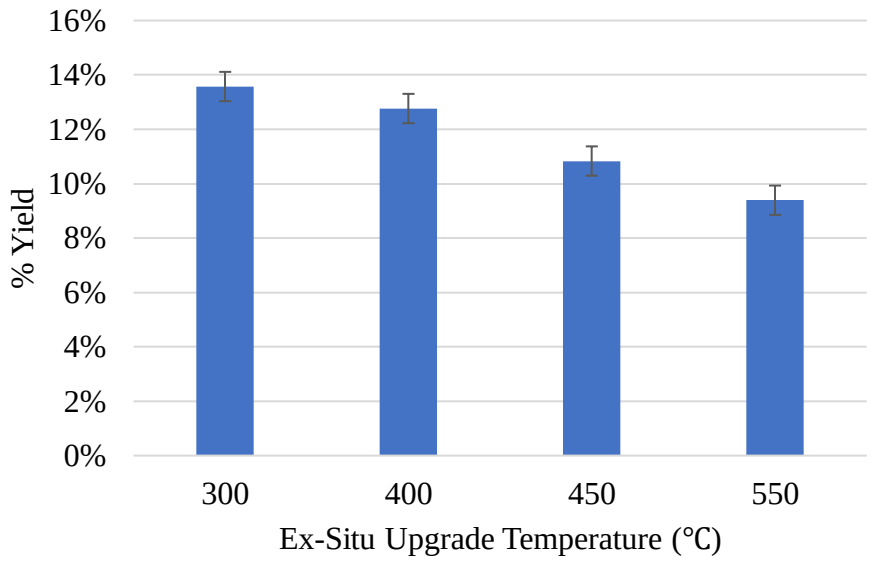

Figure 19. Yield of coke left on the catalyst as a function of ex-situ temperature.

As the temperature increased, we observed a decrease in the amount of coke left on the catalyst. We hypothesize that this is also in response to an increase in the amount of thermal cracking, and that the elevated temperature favored desorption from the catalyst active sites before oligomerization could occur resulting in less coke.[15] We also analyzed the remainder of the light oil fractions that were not collected in the methanol bubblers but in the ice bath collectors before the condenser, in a GC-MS/FID and found no significant compounds. Conducting CHN analysis of the remaining oil fractions showed that the sample consisted of approximately 10 % hydrogen with very small amount of carbon (< 1 %). Considering that biomass is mostly composed of carbon, hydrogen, and oxygen, the remainder of the sample was likely oxygen that the CHN could not detect (Figure 20). Based off of the GC/MS-FID analysis, the consistency of the oil and the CHN results, we concluded that a majority of the light oil fraction was water. This is consistent with the results from the CHN, because hydrogen is approximately 10 % the mass of water, and the other 90 % is oxygen. As temperature increases there is an observable decrease in carbon and

hydrogen content in the light oil fraction, indicating that secondary cracking reactions could have occurred leading to more small non condensable gases and decreasing the overall carbon content in the light oil fraction.

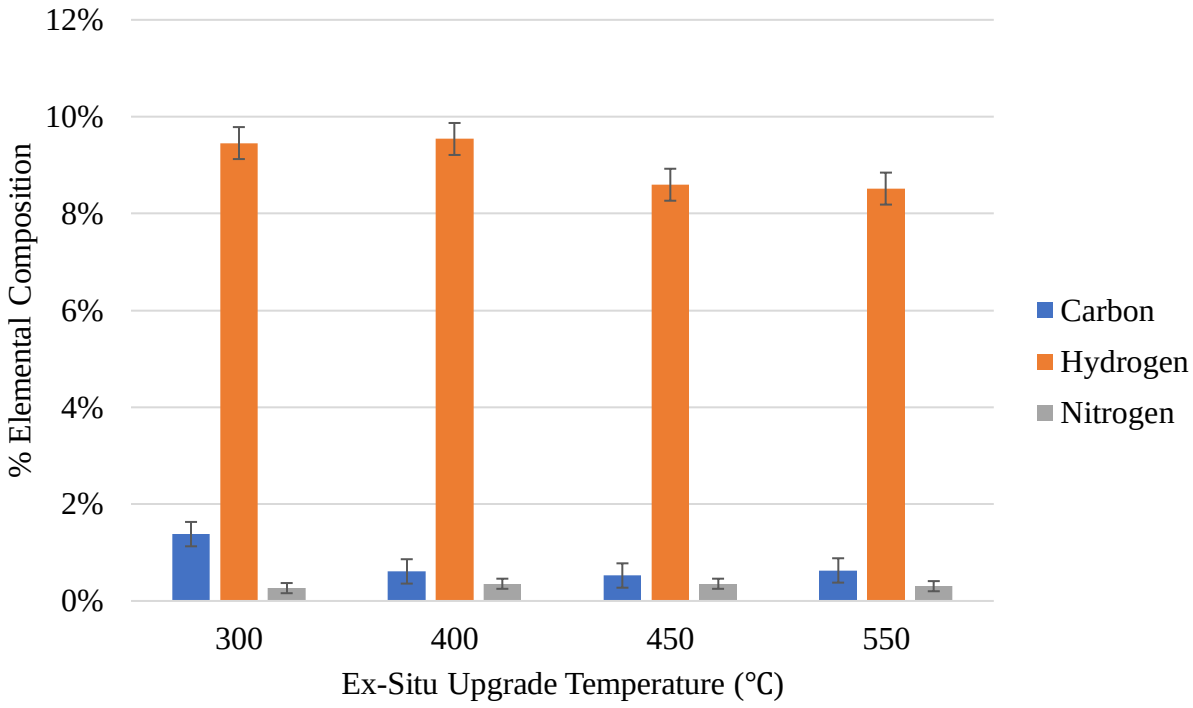

Figure 20. Elemental analysis of light oil samples as a function of temperature.

In an attempt to further close the mass balance and understand the reactions taking place in the upgrade reactor, non-condensable gases were collected for a single run at an upgrade temperature of 550℃. While we did not conducted a temperature study of gases due to the difficulty of collection, a single run produced the results seen in Figure 21. Carbon monoxide was produced in high concentration, which is typical of deoxygenation mechanisms.[38] Methane was the second gas produced in largest yields, strengthening the hypothesis of the thermal demethylation of substituted aromatics into benzene rings. The addition of the gases for that single run brings the mass balance up to 94% accounting for all liquid, solid, and gas fractions.

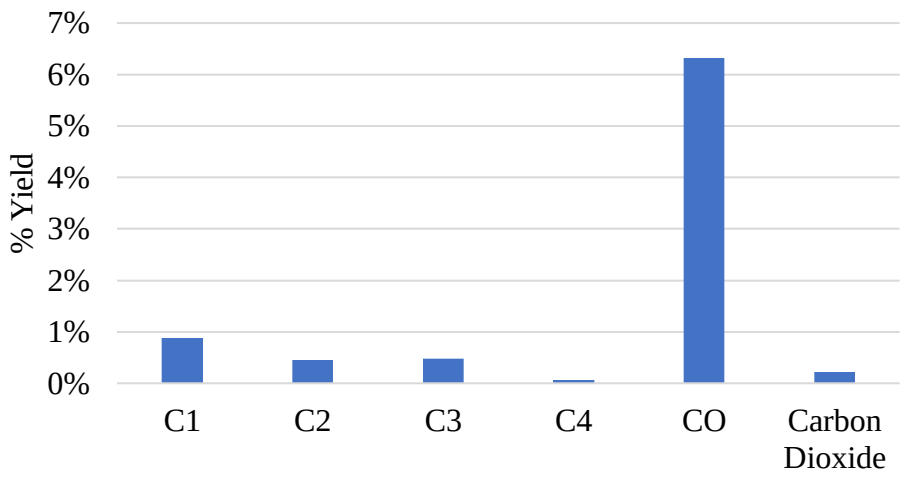

Figure 21. TCD analysis of gases collected from ablative catalytic fast pyrolysis run at a catalyst to biomass ratio of 4:1, with an ex-situ temperature of 550 ℃.

3.3.2 Catalyst to Biomass Ratio Study

We conducted a catalyst-to-biomass ratio to study verify its effects on aromatic yield. Three different ratios of catalyst to biomass were prepared (2:1, 4:1, 8:1) and tested at an *ex-situ* upgrade temperature of 550 ℃, as this produced the highest aromatic yield from the temperature screening study (Figure 22). Unfortunately, the changes in the ratios were limited by the design of the reactor system. The default catalyst to biomass ratio used was 4:1 (with 50 g of biomass). To achieve a catalyst to biomass ratio of 2:1, the length of the catalyst bed had to be shortened. Biomass could not have been added in the reactor to achieve a lower ratio using the same mass of catalyst, because of the ablative pyrolysis design. Increasing the biomass past 50 g would have resulted in slow pyrolysis at the bottom of the wood chip layer resting in the bowl, limiting the condensable volatiles yield and, increasing the char. To achieve a ratio of 8:1, the biomass had to be decreased to 25 g, rather than increasing the amount of catalyst, because the upgrade reactor has a limited volume and would not accommodate more than 230 g. Figure 22 shows that there was no significant difference in the aromatic yield for the ratios of 4:1 and 8:1. However, when the ratio

dropped to 2:1, a significant decrease in aromatic yield from 3.5 wt% to 3.0 wt% was observed. This decrease in aromatic yield with a lower ratio could be due to the decreased availability in catalyst acid sites.

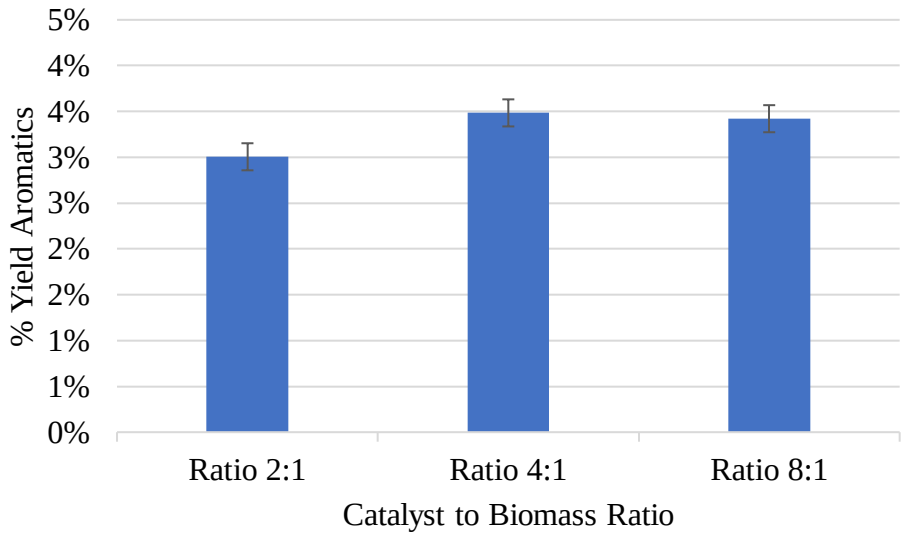

Figure 22. Yield of aromatic hydrocarbons as a function of catalyst to biomass ratio.

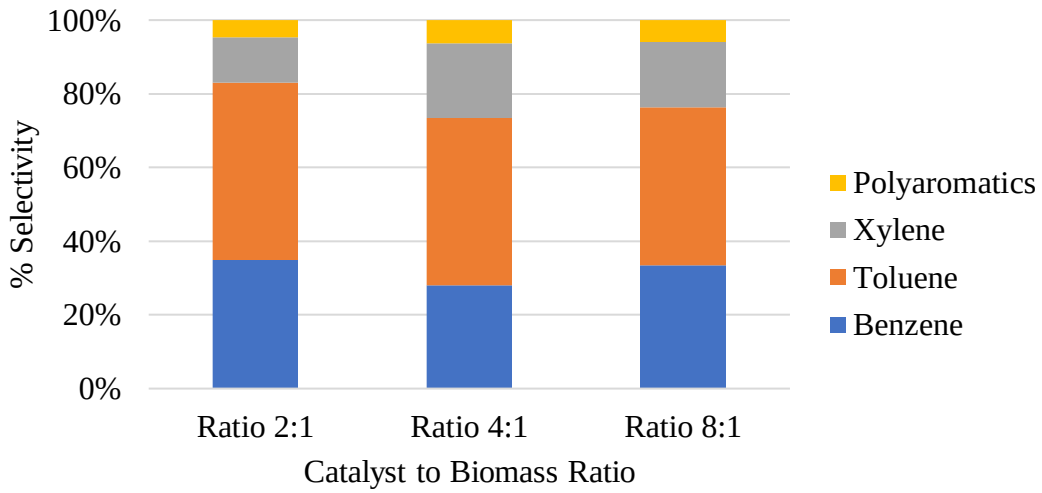

Figure 23. Selectivity of aromatic hydrocarbons for varying catalyst to biomass ratios.

Figure 23 shows that there were no significant differences in the selectivity of benzene, xylene, and toluene when varying the catalyst to biomass ratio. The mass balances of the different experimental ratios are shown in Figure 24. The increase in light oil and overall mass balance for

the ratio of 8:1 is most likely because of the small amount of biomass used, making the fast pyrolysis more effect because of the smaller amount of biomass layer in the bowl. The smaller amount of biomass would also result in less oil for the condensing system to cool down, allowing for all of the oil produced to be exposed to cooler temperatures increasing the mass balance yield.

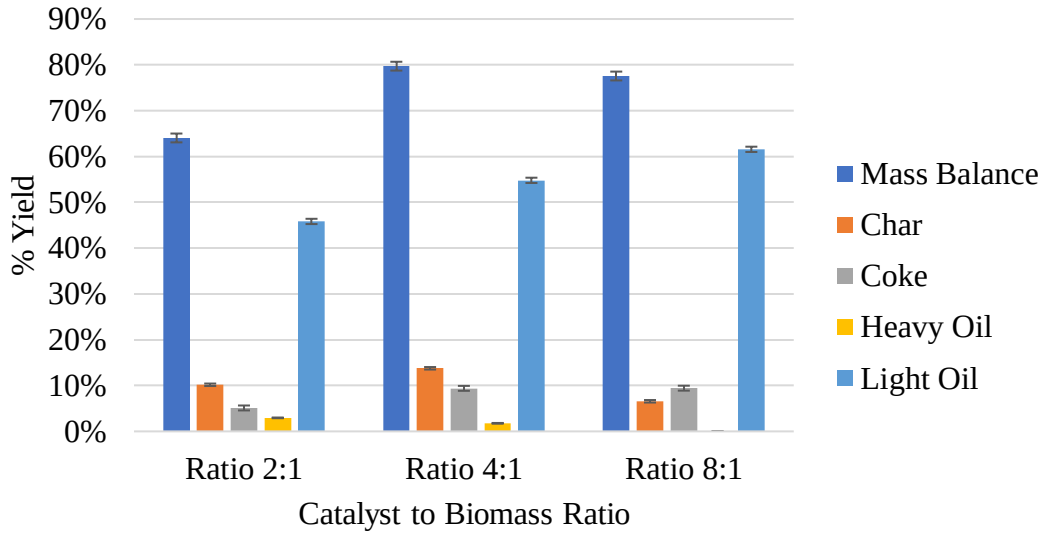

Figure 24. Mass balance breakdown for varying catalyst to biomass ratios.

The light oil fractions were also tested in the GC/MS-FID with no identifiable compounds, so we did CHN to determine the carbon, hydrogen, and oxygen content (Figure 25). We found a majority of the light oil to be water with all ratios showing very low carbon percentages. The decreasing trend in the carbon percent with increasing hydrogen content from ratio 2:1 to 4:1 is likely because of unreacted heavy oxygenated products in the 2:1 light oil fraction because of the decreased amount of acid sites available for deoxygenation as well as the increased weigh hourly space velocity. This is consistent with the lower amount of aromatic hydrocarbons produced.[24,39]

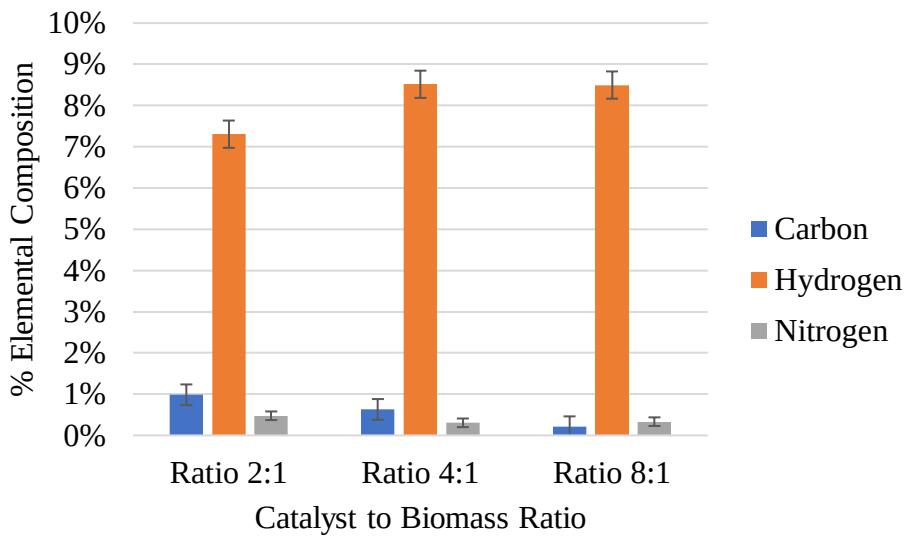

Figure 25. Elemental analysis results of different catalyst to biomass ratios.

When considering the catalyst to biomass ratio, it is also critical to consider the weight hourly space velocity (WHSV), especially in varying catalyst mass and bed length, as done here. The weight hourly space velocity was calculated using equation 3 and all WHSV were normalized by length of catalyst bed. The flow of reactants was determined by taking the mass of reacted wood and dividing by 3 minutes, and the mass flow rate of reactants from fast pyrolysis was assumed constant across the three minutes of fast pyrolysis (Equation 4). WHSV values for each catalyst to biomass ratio are shown in Table 4.

$$WHSV = \left(\frac{Mass\ flow\ rate\ of\ reactants}{Mass\ of\ catalyst\ in\ reactor}\right) \quad (3)$$

$$Mass\ flow\ rate\ of\ reactants = \frac{Mass\ of\ reacted\ wood\ (g)}{3\ minute\ fast\ pyrolysis} \times 60\ min \quad (4)$$

Table 4. Weight hour space velocities (WHSV) for each catalyst to biomass ratio.

Catalyst to Biomass	WHSV ($hour^{-1}$ cm^{-1})
2:1	.12
4:1	.066
8:1	.036

As the weight hour space velocity changes, the contact time of volatiles to the catalyst and potential active sites also changes because of the fixed bed diameter. The significant decrease in aromatics that resulted from the 2:1 ratio is most likely because of decreased exposure to catalyst active site. The reactant molecules have less exposure to active sites because there is less catalyst per biomass and the length of the bed was shortened by approximately 17.4 cm, increasing the weight hourly space velocity. The catalyst to biomass ratio of 4:1 produced the same amount of volatile aromatics as the 8:1 ratio, suggesting that the acid site availability was no longer a limiting factor. However, when we examine the amount of coke between the three catalyst-to-biomass ratios, we see that the weight hourly space velocity might be the limiting factor at the highest ratio. Although the same amount of volatile aromatics were produced, we see a significant increase in the coke resulting from the ratio 8:1, suggesting that the decreased WHSV could increase exposure time to the catalyst, thus promoting coke formation and limiting the amount of deoxygenated aromatics (Figure 24).[11]

When conducting CHN analysis of the coke, samples were mixed and ground up using a mortar and pestle to create a uniform sample. However, when the catalyst is removed from the bed, there appears to be three different layers that form from the top of the packed bed downward.

In order to understand how coke is formed throughout the catalyst bed, BET was performed on the three differently colored fractions collected from a single 4:1 ratio run at 550 ℃.

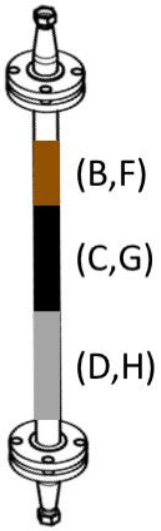

A

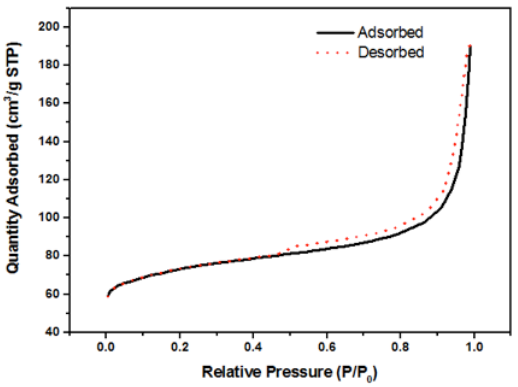
Adsorbed
Desorbed
Quantity Adsorbed (cm³/g STP)
Relative Pressure (P/P₀)

E

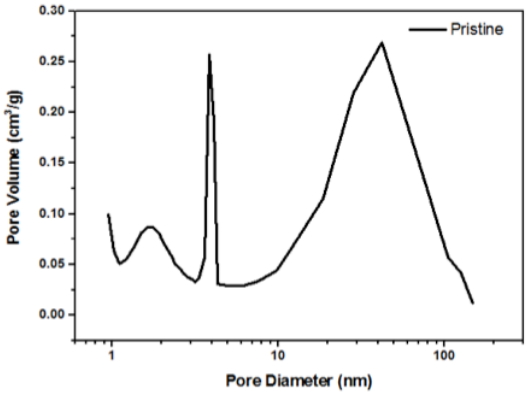
Pristine
Pore Volume (cm²/g)
Pore Diameter (nm)

B

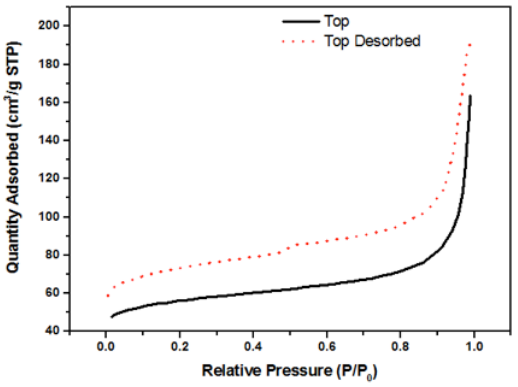
Top
Top Desorbed
Quantity Adsorbed (cm³/g STP)
Relative Pressure (P/P₀)

F

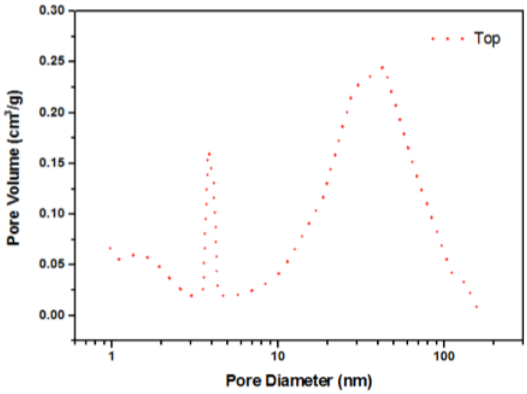
Top
Pore Volume (cm²/g)
Pore Diameter (nm)

C

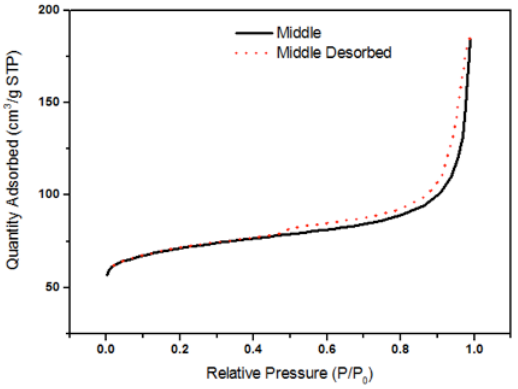
Middle
Middle Desorbed
Quantity Adsorbed (cm³/g STP)
Relative Pressure (P/P₀)

G

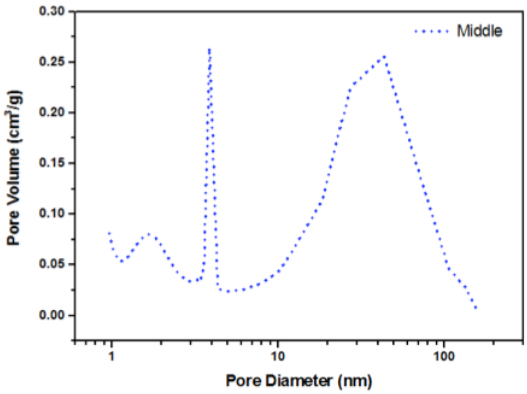
Middle
Pore Volume (cm²/g)
Pore Diameter (nm)

D

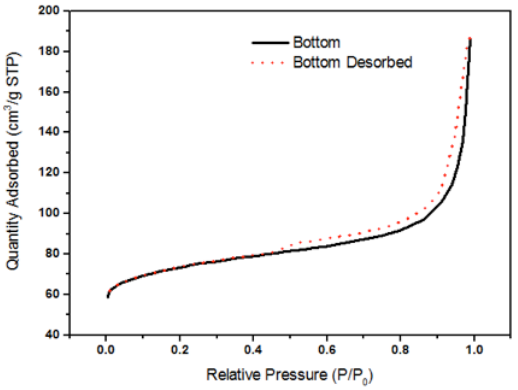
Bottom
Bottom Desorbed
Quantity Adsorbed (cm³/g STP)
Relative Pressure (P/P₀)

H

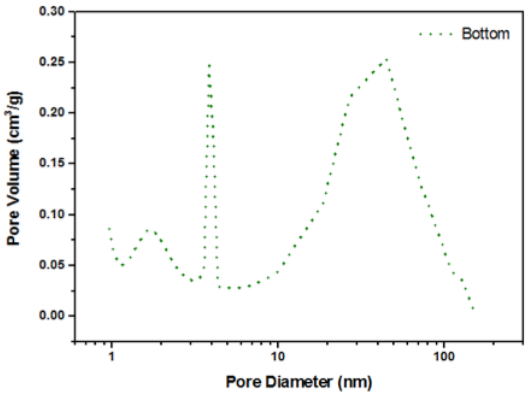
Bottom
Pore Volume (cm²/g)
Pore Diameter (nm)

Figure 26. Visual representation of color layers from packed bed upgrade reactor.(A,E) Isotherm and pore distribution diagram for fresh catalyst heated in nitrogen at 550 ℃. (B,F) Isotherm and pore distribution diagram for brown colored reacted catalyst collected.

The original catalyst is microporous and light gray in color with a surface area of 275 m^2/g (Figure 26 A,E). If we compare the isotherms for the blank and all three portions collected from the reactor, there is no difference in isotherm shape, demonstrating that the material structure was not altered or damaged in any way. The top portion of the packed bed reactor when removed had a brownish tint resembling the color of heavy bio-oil. Comparing the isotherm of the top spent catalyst to the fresh catalyst there is a decrease in overall quantity adsorbed at all relative pressures, demonstrating a decrease in surface area to 211 m^2/g (Figure 26 B,F). The pore distribution diagram also shows a decrease in the microporous volume from 182 cm^3/g to 142 cm^3/g, for the fresh catalyst and spent catalyst respectively, as well as a decrease in smaller mesopores. The middle section of the packed bed reactor has a very dark black color characteristic of catalyst coke. The isotherm shows a small decrease in overall quantity of adsorbed nitrogen, giving a surface area of 268 m^2/g. However, the surface area is still much greater than the top portion of the bed. The porosity distribution diagram mirrors this with a slight decrease in micropore volume and no change in the mesopores (Figure 26 C,G). The bottom portion of the packed bed reactor is a very light grey color similar in color to the unreacted catalyst and has no significant reduction in surface area (275 m^2/g). There is also no significant differences in porosity between the fresh catalyst and the catalyst collected at the bottom of the packed bed (Figure 26 D,H). From these changes in surface area and porosity, we conclude that a majority of the coke is formed at the top of the packed bed, with some coke formed in the middle, and little to no coke formed at the bottom of the upgrade reactor. The maintained surface area and porosity at the bottom of the bed also suggests that at a

ratio of 4:1, there is still a significant amount of catalyst available for deoxygenation. From the catalyst to biomass ratio study, we concluded that the most effective ratio was 4:1.

CONCLUSION

Fast pyrolysis of biomass is a method of creating a liquid fuel called bio-oil, but this bio-oil is not readily compatible with existing infrastructure. For this reason, it is necessary to investigate methods to upgrade bio-oil, turning it in to chemical compounds that closely resemble the make-up of gasoline, like aromatic hydrocarbons. Here, two methods of upgrade were investigated: the placement of metal nanoparticles on the surface of the wood structure to act as a catalyst, and the downstream upgrade of oxygenated volatiles produced from fast pyrolysis using a catalyst.

The deposition of palladium metal nanoparticles on wood resulted in a catalytic effect seen in the primary reactions, in which thermally stable polymers such as lignin were broken down, further increasing selectivity to phenols. These phenols are known precursors to the formation of monoaromatic hydrocarbons during catalytic upgrade.[12]While the palladium did not result in a direct conversion of organic volatiles to aromatic hydrocarbons, it presents an opportunity to increase the yield of aromatic hydrocarbons with the use of a catalyst, perhaps in the *ex-situ* method.

We also modified an existing ablative fast pyrolysis unit to include a downstream *ex-situ* upgrade reactor and a new collection system for the desired aromatic hydrocarbons. Temperature screenings were conducted on the *ex-situ* reactor to determine how varying the temperature effected aromatic yield. It was determined and recommended from the study that a temperature of 550 ℃ for the upgrade reactor should be used for the highest aromatic yield. A catalyst-to-biomass ratio study was also conducted to better understand how varying the availability of active site and

exposure to those active sites might affect aromatic yield. It was found that for this reactor design, a catalyst to biomass ratio of 4:1 results in the highest aromatic yield and lowest coke yield, and is therefore recommended for future runs.

This work contributes to the field of catalytic fast pyrolysis by examining the creation of aromatic precursors from an applied perspective by altering the biomass material, and creating a large scale *ex-situ* upgrade of those aromatic precursors.

FUTURE WORK

Future work for this study involves further work on the palladium impregnated wood as well as a catalyst screening in the ablative reactor system. While the palladium wood did not produce any aromatic hydrocarbons in the presence of atmospheric helium, the use of hydrogen at varying pressures could directly result in aromatic hydrocarbons from the palladium BKLP, rather than just precursors. Palladium is commonly used in combination with a pressurized hydrogen atmosphere to increase hydrogenation and hydrocarbon yield output.[40]

The future of the ablative reactor system involves screening studies to determine the effect of weight hourly space velocity on aromatic hydrocarbon yield. There is also an opportunity to increase the aromatic yield by adding metal ions to the HZSM-5 and trying other catalysts. There have been microscale studies with the use of gallium impregnated HZSM-5 to increase aromatic yield.[41] Catalytic fast hydropyrolysis would also be valuable in increasing the aromatic hydrocarbon yield. While a hydrogen flow would be difficult to maintain in this reactor set up, co-feeding hydrogen producing feedstocks along with BKLP could provide some sort of hydrogenation element to the upgrade.

REFERENCES

1 D. Hartman, in *Atmospheric Science Encylopedia*, Elsevier Ltd., pp. 1–46.
2 B. J. Cooke and A. L. Carroll, *For. Ecol. Manag.*, 2017, **396**, 11–25.
3 J. A. Hicke, M. C. Johnson, J. L. Hayes and H. K. Preisler, *For. Ecol. Manag.*, 2012, **271**, 81–90.
4 K. Woo, P. Watson and S. Mansfield, 2004.
5 S. Ewanick and R. Bura, *Bioresour. Technol.*, 2011, **102**, 2651–2658.
6 G. Perkins, T. Bhaskar and M. Konarova, *Renew. Sustain. Energy Rev.*, 2018, **90**, 292–315.
7 G. Luo and F. L. P. Resende, *J. Anal. Appl. Pyrolysis*, 2014, **110**, 100–107.
8 J. I. M. Arbeláez, F. C. Janna and M. Garcia-Pérez, *DYNA*, 2015, **82**, 239–248.
9 A. Bridgwater, in *Biomass Combustion Science, Technology and Engineering*, ed. L. Rosendahl, Woodhead Publishing, 2013, pp. 130–171.
10 S. Ren and X. P. Ye, *J. Anal. Appl. Pyrolysis*, 2018, **132**, 151–162.
11 P. S. Rezaei, H. Shafaghat and W. M. A. W. Daud, *Appl. Catal. Gen.*, 2014, **469**, 490–511.
12 S. Tan, Z. Zhang, J. Sun and Q. Wang, *Chin. J. Catal.*, 2013, **34**, 641–650.
13 C. A. Mullen and A. A. Boateng, *J. Anal. Appl. Pyrolysis*, 2011, **90**, 197–203.
14 S. Wan and Y. Wang, *Front. Chem. Sci. Eng.*, 2014, **8**, 280–294.
15 K. Wang, P. A. Johnston and R. C. Brown, *Bioresour. Technol.*, 2014, **173**, 124–131.
16 G. Luo and F. L. P. Resende, *Fuel*, 2016, **166**, 367–375.
17 J. Gou, Z. Wang, C. Li, X. Qi, V. Vattipalli, Y.-T. Cheng, G. Huber, W. C. Conner, P. J. Dauenhauer, T. J. Mountziaris and W. Fan, *Green Chem.*, 2017, **19**, 3549–3557.
18 Zeolite Catalysts, https://www.crcpress.com/Zeolite-Catalysts-Principles-and-Applications/Bhatia/p/book/9780849356285, (accessed June 21, 2018).
19 H. Zhang, S. Shao, R. Xiao, D. Shen and J. Zeng, *Energy Fuels*, 2014, **28**, 52–57.
20 F.-X. Collard, A. Bensakhria, M. Drobek, G. Volle and J. Blin, *Biomass Bioenergy*, 2015, **80**, 52–62.
21 S. Xing, H. Yuan, Huhetaoli, Y. Qi, P. Lv, Z. Yuan and Y. Chen, *Energy*, 2016, **114**, 634–646.
22 D. L. Dalluge, K. H. Kim and R. C. Brown, *J. Anal. Appl. Pyrolysis*, 2017, **127**, 385–393.
23 A. J. R. Hensley, Y. Wang and J.-S. McEwen, *ACS Catal.*, 2015, **5**, 523–536.
24 S. Hu, G. Yang, H. Jiang, Y. Liu and R. Chen, *Appl. Surf. Sci.*, 2018, **435**, 649–655.
25 J. Shi, M. Zhao, Y. Wang, J. Fu, X. Lu and Z. Hou, *J. Mater. Chem. A*, 2016, **4**, 5842–5848.
26 Q. Lu, M. Zhou, W. Li, X. Wang, M. Cui and Y. Yang, *Catal. Today*, 2018, **302**, 169–179.
27 F. Chen, A. S. Gong, M. Zhu, G. Chen, S. D. Lacey, F. Jiang, Y. Li, Y. Wang, J. Dai, Y. Yao, J. Song, B. Liu, K. Fu, S. Das and L. Hu, *ACS Nano*, 2017, **11**, 4275–4282.
28 J. Gu, C. Hu, W. Zhang and A. B. Dichiara, *Appl. Catal. B Environ.*, 2018, **237**, 482–490.
29 L. Zhou, S. Zhuang, C. He, Y. Tan, Z. Wang and J. Zhu, *Nano Energy*, 2017, **32**, 195–200.
30 K. Zhang, M. Shen, H. Liu, S. Shang, D. Wang and H. Liimatainen, *Carbohydr. Polym.*, 2018, **186**, 132–139.
31 Y.-S. Liu, Y.-C. Chang and H.-H. Chen, *J. Food Drug Anal.*, 2018, **26**, 649–656.
32 B. Hinterstoisser and L. Salmén, *Vib. Spectrosc.*, 2000, **22**, 111–118.

33 L. Zhou, Y. Jia, T.-H. Nguyen, A. A. Adesina and Z. Liu, *Fuel Process. Technol.*, 2013, **116**, 149–157.
34 B. Li, L. Ou, Q. Dang, P. Meyer, S. Jones, R. Brown and M. Wright, *Bioresour. Technol.*, 2015, **196**, 49–56.
35 O. D. Mante, D. C. Dayton, J. R. Carpenter, K. Wang and J. E. Peters, *Fuel*, 2018, **214**, 569–579.
36 H. Shafaghat, P. S. Rezaei, D. Ro, J. Jae, B.-S. Kim, S.-C. Jung, B. H. Sung and Y.-K. Park, *J. Ind. Eng. Chem.*, 2017, **54**, 447–453.
37 G. Luo, D. S. Chandler, L. C. A. Anjos, R. J. Eng, P. Jia and F. L. P. Resende, *Fuel*, 2017, **194**, 229–238.
38 C. Hu, R. Xiao and H. Zhang, *Bioresour. Technol.*, 2017, **243**, 1133–1140.
39 H. Zhang, M. Luo, R. Xiao, S. Shao, B. Jin, G. Xiao, M. Zhao and J. Liang, *Bioresour. Technol.*, 2014, **155**, 57–62.
40 O. Jan, R. Marchand, L. C. A. Anjos, G. V. S. Seufitelli, E. Nikolla and F. L. P. Resende, *Energy Fuels*, 2015, **29**, 1793–1800.
41 S. Vichaphund, D. Aht-ong, V. Sricharoenchaikul and D. Atong, *Renew. Energy*, 2015, **79**, 28–37.